

56-3-93
9647
NACA TN 3359 1496

0066172

TECH LIBRARY KAFB, NM

NATIONAL ADVISORY COMMITTEE FOR AERONAUTICS

TECHNICAL NOTE 3359

AN INVESTIGATION OF DRAINS DISCHARGING LIQUID
INTO SUBSONIC AND TRANSONIC STREAMS

By Allen R. Vick and Frank V. Silhan

Langley Aeronautical Laboratory
Langley Field, Va.



Washington
March 1955

AFMDC

TECHNICAL LIBRARY



TECHNICAL NOTE 3359

AN INVESTIGATION OF DRAINS DISCHARGING LIQUID

INTO SUBSONIC AND TRANSONIC STREAMS

By Allen R. Vick and Frank V. Silhan

SUMMARY

Results of an investigation of the characteristics of drains discharging liquid into an airstream at Mach numbers from 0.5 to 1.3 are presented herein. The data are presented in the form of surface stain patterns, schlieren photographs of the flow, and drag measurements for drains of circular, elliptical, and airfoil cross-sectional shapes. Variables whose influence have been investigated include Mach number, liquid reservoir pressure (referenced to free-stream static pressure), drain extension, angle of sweep, and end shape.

The predominant factors in preventing the discharging liquid from flowing back on the surface are angle of sweep and drain extension into the airstream. Pressure on the discharge liquid was of only secondary significance. These data show substantial decreases in drag coefficient as the sweep angle is increased. Lowest drag and a stain-free surface were obtained for 60° swept drain configurations.

INTRODUCTION

The desirability of knowing the path of a liquid leaving a drain was discussed as early as 1929 (refs. 1 and 2). Later analyses of airplane fire records and ways to prevent these fires (refs. 3 and 4) showed, as would be expected, that an extremely high percentage of fires could be traced either directly or indirectly to the fuel system. Long-range high-speed aircraft carrying large quantities of fuel have intensified the problems associated with dumping of fuel in emergencies, and, even under normal operating conditions, numerous drains must be provided to eliminate excess oil or loose fuel drippings from the aircraft. It is desirable to have these discharged liquids clear the surface to eliminate staining and reduce the fire hazard. At present, specific information on drains in the high subsonic or transonic Mach number range is not available.

The purpose of this investigation was to determine, over a Mach number range from 0.5 to 1.3, the characteristics of numerous drain configurations. Safety considerations dictated the use of water rather than oil or gasoline in conducting these experiments, with a water-soluble dye added to facilitate the tracing of any liquid which might reach the surface. The effects of liquid volatility and viscosity have not been explored; however, it appears improbable that the general conclusions reached would be significantly altered by differences in characteristics of these liquids. In all these tests, the drains were installed in a stream with a negligible pressure gradient. The boundary-layer thickness in the vicinity of the outlets was approximately $1/8$ inch.

Results are presented in the form of surface stain patterns, schlieren photographs, and drag data (with and without liquid flow) over a Mach number range from 0.5 to 1.3, and a liquid-reservoir-pressure range (referenced to the free-stream static pressure) from 0 to 50 lb/sq in. Reynolds number (based on the drain dimension parallel to the airstream) varied from 0.6×10^5 to 1.1×10^6 .

SYMBOLS

C_D	drag coefficient, D/qS
D	total drag, lb
d	outer diameter of drain, in.
H	total pressure from outlet, lb/sq in.
H_0	free-stream total pressure, lb/sq in.
h	projected length of drain from tunnel wall, in.
M	Mach number
P	liquid pressure differential, $P_r - p$, lb/sq in.
P_r	liquid pressure of reservoir, lb/sq in.
p	tunnel static pressure, lb/sq in.
P_v	drain-vent static pressure, lb/sq in.
Δp	difference between air-outlet static pressure and tunnel static pressure, lb/sq in.

q	free-stream dynamic pressure, lb/sq in.
S	projected frontal area of drain, sq in.
Λ	angle of sweep, deg

APPARATUS AND METHOD

The transonic research facilities used in this investigation were continuous-operation, nonreturn systems with $4\frac{1}{2}$ - by $4\frac{1}{2}$ - inch and $4\frac{1}{2}$ - by $6\frac{1}{4}$ - inch slotted test sections 17 inches in length. The general arrangement of the $4\frac{1}{2}$ - by $6\frac{1}{4}$ - inch test section is shown in figure 1 with one of the drain models in position. Drag data and schlieren photographs were obtained with the models mounted in the top floor of the $4\frac{1}{2}$ - by $6\frac{1}{4}$ - inch test section; for the stain tests, however, models were mounted in the side wall of the $4\frac{1}{2}$ - by $4\frac{1}{2}$ - inch test section (fig. 2). A check run was made in a tunnel of 100-square-inch cross-sectional area where the interference effects of tube shape would be reduced approximately 75 percent.

Geometric variables investigated include drain length (that is, projection into the airstream), angle of sweep, end shape, and cross-sectional shape (circular, elliptical, and airfoil). In addition, the effects of addition of vanes and vane angle of attack were investigated. All circular tubes had an inside diameter of 0.125 inch and an outside diameter of 0.25 inch; the outside dimensions of the ellipses were 0.54 and 0.25 inch (wall thickness of 0.0625 inch); airfoil fairings were 12-percent-thick symmetrical sections with 2-inch chords normal to the leading edge, and the internal drain dimension was the same as circular-tube internal dimension. In order to investigate the effects of an end taper on the liquid jet, the wall thickness of one circular tube was tapered a distance of $1\frac{1}{4}$ inches so that the end of the drain vent had the minimum wall thickness. This drain length was projected several feet upstream in the tunnel test section to minimize the interference effects. In order to determine the effects of a blast of air around the drain, circular drains located in air outlets of $3/8$ -inch and $7/8$ -inch diameter were also investigated. Auxiliary air flow for these outlets was supplied through a flexible hose from a bleedoff upstream of the test section. Static pressure measured in the outlet was used in defining the pressure differential between the auxiliary airstream and the free stream. A summary of all configurations is given in table I.

Stain patterns were obtained at free-stream Mach numbers of 0.5, 0.7, 1.0, and 1.3 by photographing the tunnel side wall after a water-soluble dye solution was sprayed from the models for a period of 30 seconds. The tunnel side wall was painted white to facilitate photographing. After each run the side wall was photographed, and the tunnel was shut down to clean the surface. The length of surface behind the models that could be photographed was 10 inches. Liquid for these tests was supplied from a reservoir with a variable-pressure control system and a solenoid switch for rapid flow control. Liquid pressure (referenced to the tunnel static pressure) was varied from 0 to 50 lb/sq in. The tunnel static pressure for these tests was approximately atmospheric up to $M = 1.0$; above $M = 1.0$, the total pressure remained approximately constant at 26 lb/sq in. abs. Schlieren photographs were obtained in separate runs by using a single-pass schlieren system with two parabolic mirrors and a light source furnished by a high-voltage discharge through an air-cooled mercury lamp. Mach number values on the schlieren and stain photographs are accurate to ± 0.01 , and the liquid-pressure values for the corresponding photographs are accurate to ± 0.5 lb/sq in.

Drag was measured for two conditions: first, without liquid flow, and second, with liquid flow; however, only one liquid pressure was used for the latter measurements. The drag balance was a simple cantilever system used in conjunction with a strain-gage element. The drain tubes were supported in the balance and any movement due to drag was transmitted through two flat cantilever springs to the unbonded strain gage whose output was transmitted to a recorder. Clearance between the drain tube and tunnel wall was kept small (approximately 0.005 inch), and a light was installed to warn of any contact between the two.

RESULTS AND DISCUSSION

Results of this investigation are summarized in table I, together with significant dimensions and shapes of all drain configurations tested. Under the heading of flow characteristics, the drains are rated either good or poor. A rating of good indicates that the drain discharges its liquid free of the surface (in the field of view), and a rating of poor indicates that the expelled liquid strikes the surface. The results of a particular drain test are tabulated by figure number alongside each configuration. Also presented in table I are the drag coefficients at a Mach number of 1.0 for two conditions: one is without liquid flow, and the other is with liquid flowing from the tube.

In general, straight circular drains were found to have poor flow characteristics and, as shown in table I(a), also to have the highest drag. This table shows that drag reductions, as well as improved flow characteristics, are associated with increases in sweep angle. The most

efficient circular drain tested was that with the highest sweep angle (60°), followed by a short straight section parallel with the airstream. With elliptical tubes (table I(b)), a sweep angle of 60° also resulted in lower drag. Since the tube height is the projected distance to the tube axis, changes in end shape caused differences in the value of h as indicated by the points labeled a, b, and c in the sketch of table I(b). For comparable tube projections and sweep angles, the drag coefficient for tubes of elliptical cross section was significantly less throughout the Mach number range than that of the circular tubes and was further reduced by the addition of an NACA 0012 airfoil fairing (table I(c)). The characteristics of these drains are presented in greater detail in the following sections. Additional data in the form of drain-vent pressures are presented for most of the drain configurations tested. These results are presented as a differential between the drain and free-stream static pressures.

Surface staining.- Characteristic stains produced by liquid flowing along a surface after being discharged from tubes whose axes were normal to the surface are presented in figure 3. Photographs show the side wall of the tunnel with the drain located on the center line and at the left of each picture. Flow for all configurations is from left to right. The large black circle which appears in each photograph is the removable section of the side wall in which the drain was secured. Figure 3(a) presents stain patterns produced by a flush-type drain at various Mach numbers and liquid pressures. A study of the upper left-hand photograph ($M = 0.70$ and $P = 9$ lb/sq in.) shows two dark bands, symmetrically located, leading away from the drain. The dark bands, approximately $1/4$ inch wide, originate from each side of the drain in a circular arc with its center located at the rear of the drain tube. The center section between the two bands shows only a slight discoloration or stain. Visual observations indicated that part of the liquid on the surface flowed outward toward the edge of the wake produced by the liquid jet. Comparison of the photographs in any one row shows that the effect of Mach number on the stain patterns from flush drains is negligible. Increases in liquid pressure, at a constant Mach number (top to bottom along any one column), increase slightly the total wetted area of the stain. At $M \approx 1.3$, the stained area extended a distance of approximately 1 drain diameter ahead of the drain (not visible in these pictures), thus a short field of reversed flow is indicated. The presence of this area at only the highest Mach numbers and liquid-pressure differentials suggests that the reversal in flow is probably caused by boundary-layer separation induced by the shock wave ahead of the outlet.

Extending the drain tube 1 inch (fig. 3(b)) reduced the wetted area, but further projections from 1 to 2 inches (fig. 3(c)) produced negligible changes in this area. Changes in liquid pressure appear to have little effect on the wetted area for drains normal to the airstream, but with increasing Mach number the wetted area is reduced. The intensity of the

two bands increases with each increase in drain extension. Similarity of the stain patterns above and below the plane of symmetry (figs. 3(a), (b), and (c)) indicates that the gravitational effect on the discharging liquid is negligible for the distance shown in the photographs.

A 45° chamfer on the downstream side (fig. 3(d)) had little effect on the amount of liquid reaching the surface as evidenced by the stain patterns. Addition of a single 0° vane to the chamfered end of the drain, used in an attempt to prevent the axial flow of liquid down the back of the drain (fig. 3(e)), was ineffective. Changing the angle of attack of the vane from 0° to -20° (fig. 3(f)) and the addition of a second vane at an angle of attack of -20° (fig. 3(g)) also failed to eliminate wetting of the surface.

Results obtained by discharging liquid from a drain extending $5/8$ inch normal to the surface and bent 90° with a 2-inch straight section parallel to the floor are shown in figure 3(h). At low Mach numbers, the liquid first strikes the surface several inches downstream of the drain end with pressure changes having little effect, but at $M > 1.0$, both Mach number and pressure increased the stain-free distance from the liquid discharge point. At $M \approx 1.3$ and for high pressures, the surface was clear for approximately 30 drain diameters. Increasing the drain extension to 1 inch (fig. 3(i)) resulted in slight improvements for all pressures and Mach numbers. Satisfactory results were obtained at all Mach numbers when the drain was swept 60° as is shown in figure 3(j) with a $1/2$ -inch straight section parallel to the wall.

A comparison of figures 3(i) and 3(j), in which the liquid is turned parallel to the airstream, shows the liquid striking the surface at $M \approx 0.7$ in figure 3(i) and remaining free of the surface at the same Mach number in figure 3(j). This improvement in flow characteristics produced by sweeping the tube is attributed to the cross-flow component of the air flow directed away from the surface, which carries the liquid into the stream and completely eliminates the flow down the back of the drain tube. Liquid discharged from the end of a cylindrical tube whose axis is swept rearward 60° is shown in figure 3(k) to remain free from the surface at all conditions tested.

The use of drains in conjunction with air outlets from which air was ejected around the drain is presented in figure 4. A blast of air was used in an attempt actually to blow the discharging liquid away from the surface as it tried to flow down the rear of the drain. Results of a series of tests are shown in figure 4(a) in which a $1/4$ -inch-diameter drain, projecting 1 inch into the airstream, is located in the center of a $3/8$ -inch-diameter outlet. Mach number effects at a constant liquid pressure and outlet static pressure around the drain show that both the intensity and width of the stain pattern increase as M increases from 0.5 to 1.0; however, for increases from $M \approx 1.0$ to 1.3 the stain width decreases. Increasing the liquid pressure

decreased the stain width at Mach numbers up to $M \approx 1.0$ but increased it at $M \approx 1.3$. The least stain occurred for the lowest rate of air flow. Increasing the air-outlet diameter to 7/8 inch (fig. 4(b)) failed to produce any reduction in stain pattern. Although a clear surface is evident for approximately 12 drain diameters, the stain intensity is much greater where the liquid does strike the surface. The ejection of high-pressure ($H \approx H_0$) air around 1/4-inch drain tubes extending 1 inch normal to a surface failed to eliminate staining of the surface. Figure 4(c) presents data for a 3/8-inch-diameter, 60° swept outlet with a coaxial drain and indicates unsatisfactory performance was obtained with a 1/2-inch extension (projected) of the drain tube. With a 1-inch extension (not shown), only a very slight stain is evident at subsonic Mach numbers and a completely stain-free surface is evident for $M \geq 1.0$.

The effect of allowing the liquid to drip rather than flow from tubes of 0° and 60° sweep was also investigated. In these tests, which were conducted at $M = 1.2$, 1 pint of liquid was allowed to drip from a straight ($\Lambda = 0$) circular-cross-section drain at a rate of 0.6 gallon per hour. This resulted in a very intense stain with a "Bunsen flame" type of pattern (fig. 5) which was different from the stain pattern obtained at higher liquid flow rates. The symmetrical dark bands marking the edge of the wake are still present and their width has increased. A similar test conducted at $M = 1.2$ for a sweep angle of 60° and a 1-inch drain extension resulted in a surface completely free of any stain; the flow rate for this test was 0.34 gallon per hour. Thus the results of this investigation, obtained at higher discharge flow rates, may be expected to apply generally at much lower rates of discharge.

Schlieren photographs. - To assist in the visualization of liquid flow from drains, schlieren photographs were taken to show the liquid as it leaves the drain. It will be noted that in all the schlieren pictures the drains appear to extend from the bottom of the tunnel instead of projecting from the upper floor as tested. The necessity for inverting these photographs to keep the direction of flow from left to right, as in the preceding figures, stems from the use of a schlieren system in which the light passage through the stream was from left to right. Gravitational effects have previously been shown to be negligible.

Photographs taken with a circular drain tube extending 1 inch into the airstream are presented in figure 6(a). The picture at the upper left shows liquid discharged at a very low pressure at $M = 0.5$ from the end of a tube whose axis was normal to the surface; the liquid flowed down the back side of the tube and entered the wake along the entire length of the tube. A similar stain pattern is shown in figure 3(b). It is apparent from these pictures that low pressures at the back of the drain draw the liquid into the region behind the tube and thus fill in the void resulting from separation on the cylinder. Comparison of the various photographs of figure 6(a) shows

that both Mach number and liquid pressure have a decided effect on the amount of liquid striking the surface. Increasing Mach number at constant liquid pressure increases the amount of liquid flowing down the back of the drain; this may be seen in the pictures across the figure; the amount of liquid striking the surface is decreased by increasing the liquid pressure. The normal shocks, which appear at $M = 0.70$ and $P = 1.0$ lb/sq in. (and in succeeding photographs), are attributed to intermittent disturbances which originate downstream of the test section. Photographs at $M = 1.0$ and high pressures show the liquid leaving the drain in two distinct bands - one from the end and the other which seems to originate at the base of the drain.

The effect of shock reflection on the jet spread can be established by a comparison of figures 3(b) and 6(a) at $M = 1.3$. A side view of the drain configuration at $M = 1.3$ and $P = 25$ lb/sq in. in figure 6(a) shows a shock being reflected from the liquid with no apparent effect on the jet spreading; figure 3(b) shows that this compression shock, impinging on the liquid jet, has no effect on the stain pattern. In a study of figure 6(a), it should be pointed out that only a small percentage of the shock can be seen to reflect from the liquid; most of the shock is on either side of the liquid jet.

A 45° chamfered tube was tested and the results obtained are presented in figure 6(b). Except for the fact that the liquid is more evenly distributed behind the drain, the effects due to Mach number and pressure are similar to those of the previous configuration shown in figure 6(a). A comparison of figures 6(a) and (b) at $M = 1.0$ shows the discharge characteristics for the 45° chamfered tube are such that more liquid is directed onto the surface than for the nonchamfered drain.

The influence of sweep angle is considered next, and the results at a 30° angle of sweep are presented in figure 6(c). At subsonic Mach numbers, the liquid remained clear of the surface at all pressures; at $M = 1.0$ and 1.3 , however, the liquid started to flow down the back of the drain but because of the presence of the lateral air-flow component is swept away from the surface. Reducing the drain extension by one-half (fig. 6(d)) resulted in some liquid reaching the surface at the higher Mach numbers. With the sweep angle increased to 60° (fig. 6(e)), the liquid remained free from the surface for all conditions tested. This was also observed in figure 3(k). Increasing the sweep angle produced significant decreases in the width of the liquid band (figs. 6(c) and (e)). Photographs of results produced by reducing the drain extension by 1 and then 2 drain diameters are seen in figure 6(f) and (g), respectively. Results are generally good although, for the shortest drain extension, there is some indication that a slight spray hits the surface. It is evident, therefore, that any further reduction in drain extension would prove undesirable.

With the tube axis parallel to the direction of air flow, the liquid jet spreads as shown in figure 7. With the end of the cylindrical tube cut off square, the liquid jet expanded immediately to the base diameter, but beyond that point the jet spread at a relatively slow rate. The effect of external tapering on the end of the tube for a distance of $1\frac{1}{4}$ inches as shown in figure 7(b) appears to be slight, with the maximum discharge diameter reduced and the edge of the liquid jet somewhat smoother for the streamlined drain of figure 7(b).

Schlieren photographs of flow from elliptical cylinders (2:1 axis ratio) with varying end shape and angle of sweep are shown in figure 8. In figure 8(a) results for the straight ellipse ($\Lambda = 0^\circ$) show that, for subsonic Mach numbers, the liquid will remain free of the surface for a few inches at all pressures investigated. At $M = 1.0$ and 1.3 , the flow "fill-in" of the wake region is similar to that for circular drains, especially at low pressures. It is evident that the overall results are unsatisfactory in spite of the improvement shown over circular drains with the same extension. The effect of sweeping the ellipse 30° (fig. 8(b)) shows good subsonic results but poor results at $M = 1.0$ and 1.3 . A comparison with figure 6(d) shows that ellipses have better discharge characteristics than circular tubes. Cutting the end of the drain parallel to the airstream (fig. 8(c)) produced no great changes in the flow; however, a comparison of figures 8(b) and (c) indicates that the drain with the end cut perpendicular to the drain center line produces less spray. Increasing the sweep angle to 60° (fig. 8(d)) gives excellent results. A comparison of this drain with the circular type shown in figure 6(e) shows no outstanding difference in the flow characteristics. Figure 8(e) in which the end of the ellipse was cut perpendicular to the airstream shows that this configuration failed to produce any strong changes in the flow. A further change in end shape in which the drain end is cut parallel to the airstream (fig. 8(f)) shows the liquid still flowing free of the surface. It is important to note that the projected height of the drains shown in figures 8(d), (e), and (f) decreases with each change in end shape. From a comparison of the bands of liquid shown in these three figures, it appears that, for a sweep angle of 60° , end shape has no outstanding effects on the discharge characteristics.

Flow from a 12-percent-thick symmetrical airfoil type of drain is shown in figure 9(a) for a 1-inch extension. Results are good for all Mach numbers and pressures, with best results at high Mach numbers. The spray effect of the liquid increases with increases in pressure and decreases with increases in Mach number. At $M = 1.3$, the width of the discharge band appears to be at a minimum. From the results presented herein, it is important to note that this type of drain is the only drain projected normal to the free stream that has proven satisfactory at all Mach numbers. The effects of sweep on an airfoil drain are shown in figure 9(b). Spray effects as shown by the size of the liquid

band are reduced considerably by the increase in sweep angle. A comparison of figures 9(b) and 8(c) in which the end of the drain was parallel to the airstream shows the spray effects to be greater for the elliptical drain than for the NACA 0012 profile.

Drag coefficient.- Drag curves are presented in figures 10 to 12. In each case the coefficients, based on the frontal area of the tube, are presented for two conditions; one, without liquid flow and the other, with liquid discharging at a pressure differential of approximately 15 lb/sq in. Differences between these curves are attributed to the thrust component of the liquid discharged and to changes in flow patterns about the tube itself; however, no attempt has been made to separate these two effects.

Drag coefficients as a function of stream Mach number in the range from 0.5 to 1.3 for a straight circular drain extending 2 diameters from the wall are presented in figure 10(a). The dip in the drag curve in the Mach number range from 1.0 to 1.25, present in most of these tests, is attributed to tunnel-wall interference; the dashed line which bypasses this region is considered more representative than the line through the data points. This wall interference is attributed to reflection of the bow shock from the tunnel side wall; the pressure rise across the shock transmitted through the wake increases the pressure at the back of the drain and thus reduces the drag. As the Mach number is increased, the reflected shock moves farther downstream and its influence disappears. With liquid flowing from the drain, the drag at all Mach numbers is decreased substantially. This result, contrary to that obtained by Rogallo when air was discharged through a similar tube at $M \approx 0.1$ (ref. 5), is due to an effective streamlining of the body by the presence of large amounts of liquid in the wake of the tube. In figure 10(b), the drain extension has been increased to 1 inch ($h/d = 4$). The slope of the drag curve is increased considerably in the subsonic Mach number range, and above $M = 1.0$, the drag coefficient is substantially greater than that obtained with the shorter tube. Over a Mach number range from $M = 1.0$ to 1.3 results show that, for values of h/d less than 4, the slope of the drag curve is positive, and for values greater than 4, the slope is negative. A similar result has been obtained in flight by the use of tubes with much greater values of h/d (ref. 6). Effects of a 45° chamfer on the drag characteristics of a drain are shown in figure 10(c). A slight reduction in C_D is observed at subsonic speeds, but in the transonic range the difference becomes negligible. As in previous cases, the presence of the liquid jet reduces the drag significantly.

Data shown in figure 10(d) were obtained with the drain tube extending normal to the wall with a 90° elbow to discharge liquid

parallel to the airstream. With this configuration, the drag coefficients both with and without liquid flow were substantially less than those obtained with straight tubes; Rogallo also showed lower drag coefficients with this type of installation (ref. 5). With the drain extension increased to 1 inch (fig. 10(e)), an unexpected dip appears in the Mach number range between $M = 0.7$ and 0.9 . Examination shows that the data above $M = 0.9$ are comparable with previous data; it therefore appears that the subsonic data below $M = 0.9$ are affected by the bend in the tube and the straight section. Reference 6 showed similar dips for cylinders with very high values of h/d with the dips disappearing as h/d was reduced. The drag curve of figure 10(e) is comparable to that obtained in reference 6 with an h/d of approximately 30.

Drag coefficients obtained with tubes swept 30° are presented in figures 10(f) and 10(g) and swept 60° in figures 10(h) to 10(k). These curves show that increasing the sweep produces large reductions in drag coefficient and indicate substantial reductions in the effect of the liquid jet throughout the Mach number range. The latter effect was smaller for larger tube extensions. The magnitude of the jet effect is much greater than its thrust component alone, and indicates substantial improvement in the air flow around the tube itself.

With the stem of the drain tube swept rearward 60° and with a 1/2-inch length of tube parallel to the airstream (fig. 10(h)), the drag coefficients both with and without liquid flowing were reduced to approximately one-half the values shown in figure 10(e). The small drag decrease obtained with liquid being discharged from the tubes approximates the thrust of the liquid jet. This thrust amounts to 1.3 ounces when a similar jet of water is discharged into the atmosphere.

The improvement of drag characteristics obtained by changing from circular to elliptical tubes is shown by comparison of the drag coefficients presented in figure 11 with those in figure 10. In figure 11(a) a straight ellipse with a 1-inch extension shows a definite decrease in C_D relative to that obtained with the circular drain (fig. 10(b)) and a reduction in the drag difference between flow and no-flow conditions. With elliptical profiles the slope of the drag curve at subsonic Mach numbers increases at a higher rate than for the circular drains, and the drag rise near $M = 1.0$ is less pronounced. In addition, as in the previous tests, sweeping the tube axis rearward (fig. 11(b)) reduced the drag coefficients at all Mach numbers. Figures 11(b) and (c) show a negligible difference in C_D resulting from changing the plane in which the 30° tube was cut off. With the tube axis swept 60° , however (figs. 11(d), (e), and (f)), appreciably higher transonic drag coefficients were measured with the tube cut off in a plane parallel to the tunnel wall.

Drag coefficients for a straight 12-percent-thick symmetrical airfoil drain with a span of 1 inch are shown in figure 12(a). General reductions in C_D over circular and elliptical drains are noted throughout the Mach number range. The curve for tests with liquid flow conditions shows that the drag coefficient is higher at subsonic speeds than the drag coefficient with no flow. This result is a reversal of previous trends. This higher drag coefficient for subsonic flow is probably caused by the liquid trailing over the rear section of the airfoil, and this liquid flow increases the effective thickness of the body. The higher pressure in the region behind the local shock at $M > 0.93$ results in a decrease in drag on the thicker body and hence lower drag at transonic speeds. Sweeping the airfoil rearward 30° (fig. 12(b)) produced an average decrease of approximately 25 percent in the drag coefficient.

Vent pressures.- In figure 13, the drain-vent pressure data at no-liquid-flow conditions for various tube configurations are presented as $\frac{p_v - p}{q}$ plotted against Mach number. A characteristic dip present in the curves between $M = 0.9$ and 1.0 also appeared for the check run in a 100-square-inch tunnel where interference effects were reduced 75 percent. The break in the curves at about $M = 1.15$ is related to wall reflection of shocks as discussed in the preceding section on drag results. In general, an increase in length from 2 to 4 diameters for the tubes with the axis normal to the surface decreased the vent pressure. Increasing the angle of sweep to 30° and then to 60° with the drain extension remaining constant produced an increase in vent pressure. With elliptical- and airfoil-shaped drains, the drain-vent pressures were closer to free-stream pressure than with drains of circular cross section. Sweepback of the elliptical drains produced no significant change. Varying the tube cutoff from a plane parallel to the wall to one perpendicular to the wall or the tube axis in general increased the pressure decrement.

CONCLUSIONS

Results of the characteristics of drains discharging liquid into an airstream at Mach numbers from 0.5 to 1.3 have been studied, and these results lead to the following conclusions:

1. Within the range of these tests, surface staining cannot be avoided with liquid being discharged from tubes of circular or elliptical cross sections extending normal to the surface. An airfoil-shaped drain which was unswept was satisfactory.

2. Surface staining could, in many cases, be eliminated throughout the Mach number range by sweeping the tubes rearward. No wetting of the surface was encountered within the 10-inch length of surface available, when the tubes of circular and elliptical cross section were swept as much as 60° .

3. Air flow around drains located in auxiliary air outlets failed to prevent wetting of the surface for either normal or swept configurations.

4. Vent pressures (for no liquid flow) for drains which project either normal to, or parallel to, the airstream decrease with increasing drain extension and increase with increasing sweep angle.

Langley Aeronautical Laboratory,
National Advisory Committee for Aeronautics,
Langley Field, Va., July 19, 1954.

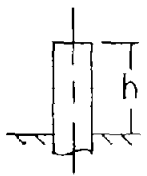


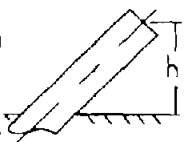






REFERENCES

1. Sabatier, J.: Fire Prevention on Airplanes. Pt. II. NACA TM 537, 1929.
2. Brunat, Henri: Combating Airplane Fires. NACA TM 550, 1930.
3. Pesman, Gerard J.: Analysis of Multiengine Transport Airplane Fire Records. NACA RM E9J19, 1950.
4. Glendinning, W. G., and Drinkwater, J. W.: The Prevention of Fire in Aircraft. Jour. R.A.S., Vol. 51, No. 439, July 1947, pp. 616-641.
5. Rogallo, F. M.: Internal-Flow Systems for Aircraft. NACA Rep. 713, 1941.
6. Welsh, Clement J.: The Drag of Finite-Length Cylinders Determined From Flight Tests at High Reynolds Numbers for a Mach Number Range From 0.5 to 1.3. NACA TN 2941, 1953.

TABLE I.- SUMMARY OF CONFIGURATIONS TESTED AND DATA OBTAINED

14

(a) Circular drains - 0.25-inch O.D., 0.125-inch I.D.

	h, in.	Sweep angle, deg	Flow character- istics (all Mach numbers)	C_D ($M = 1.0$)		C_D in figure	Stain pattern in figure	Schlieren photo in figure
				.5	1.0			
	0	0	Poor			—	3(a)	—
	0.50	0	Poor			10(a)	—	—
	1.0	0	Poor			10(b)	3(b)	6(a)
	2.0	0	Poor			—	3(c)	—
	0.50	60	Good			10(k)	—	6(g)
	0.75	60	Good			10(j)	—	6(f)
	1.0	60	Good			10(i)	3(k)	6(e)
	0.87	30	Poor			10(g)	—	6(d)
	1.73	30	Poor			10(f)	—	6(c)
	1.0	0	Poor			—	4(a)	—

NACA TN 3559

TABLE I.- SUMMARY OF CONFIGURATIONS TESTED AND DATA OBTAINED - Continued

(a) Concluded



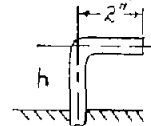




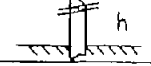
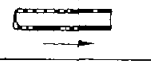
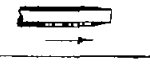

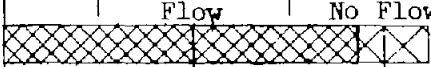
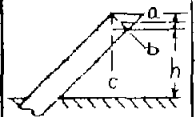





	h, in.	Sweep angle, deg	Flow character- istics (all Mach numbers)	C_D ($M = 1.0$)			C_D in figure	Stain pattern in figure	Schlieren photo in figure
				.5	1.0				
	1.0	0	Poor				—	4(b)	—
	0.50	60	Poor				—	4(c)	—
	1.0	60	Poor				—	—	—
	0.63	0	Poor	Flow No Flow			10(d)	3(h)	—
	1.0	0	Poor				10(e)	3(i)	—
	1.0	60	Good				10(h)	3(j)	—
	1.0	0	Poor				10(c)	3(d)	6(b)
	1.0	0	Poor				—	3(e)	—
	1.0	0	Poor				—	3(f)	—
	1.0	0	Poor				—	3(g)	—
	—	90	—				—	—	7(a)
	—	90	—				—	—	7(b)

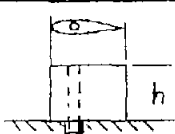

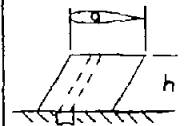

TABLE I.- SUMMARY OF CONFIGURATIONS TESTED AND DATA OBTAINED - Concluded

16

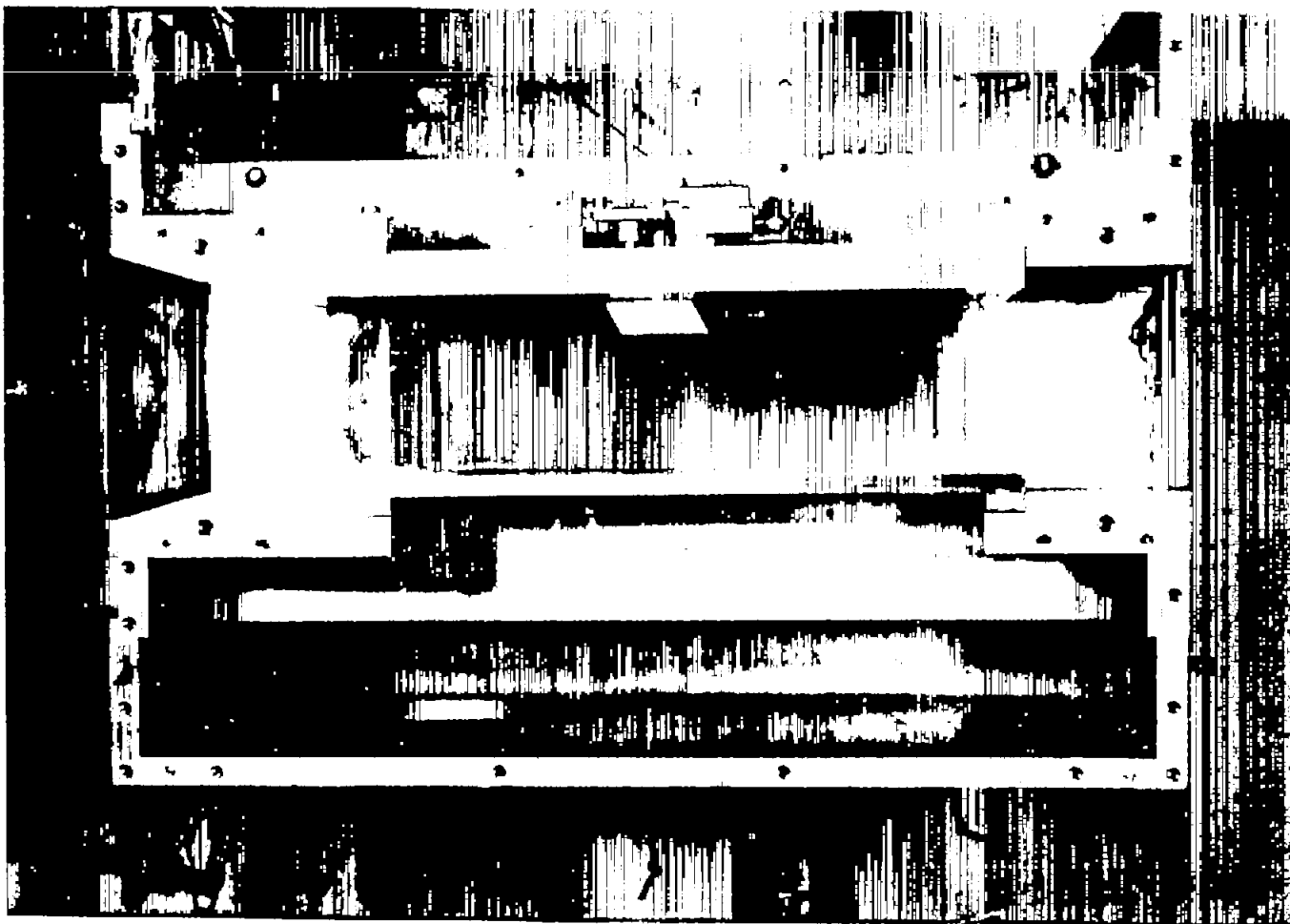
(b) Elliptical drains - fineness ratio 2:1

	h, in.	Sweep angle, deg	Flow character- istics (all Mach numbers)	C_D (M = 1.0)		C_D in figure	Stain pattern in figure	Schlieren photo in figure
				.5	1.0			
	1.0	0	Poor			11(a)	—	8(a)
	0.75 (a)	30	Poor			11(c)	—	8(c)
	0.87 (b)	30	Poor			11(b)	—	8(b)
	0.63 (a)	60	Good			11(f)	—	8(f)
	1.0 (b)	60	Good			11(d)	—	8(d)
	0.93 (c)	60	Good			11(e)	—	8(e)

(c) Airfoil drains - 12 percent thick

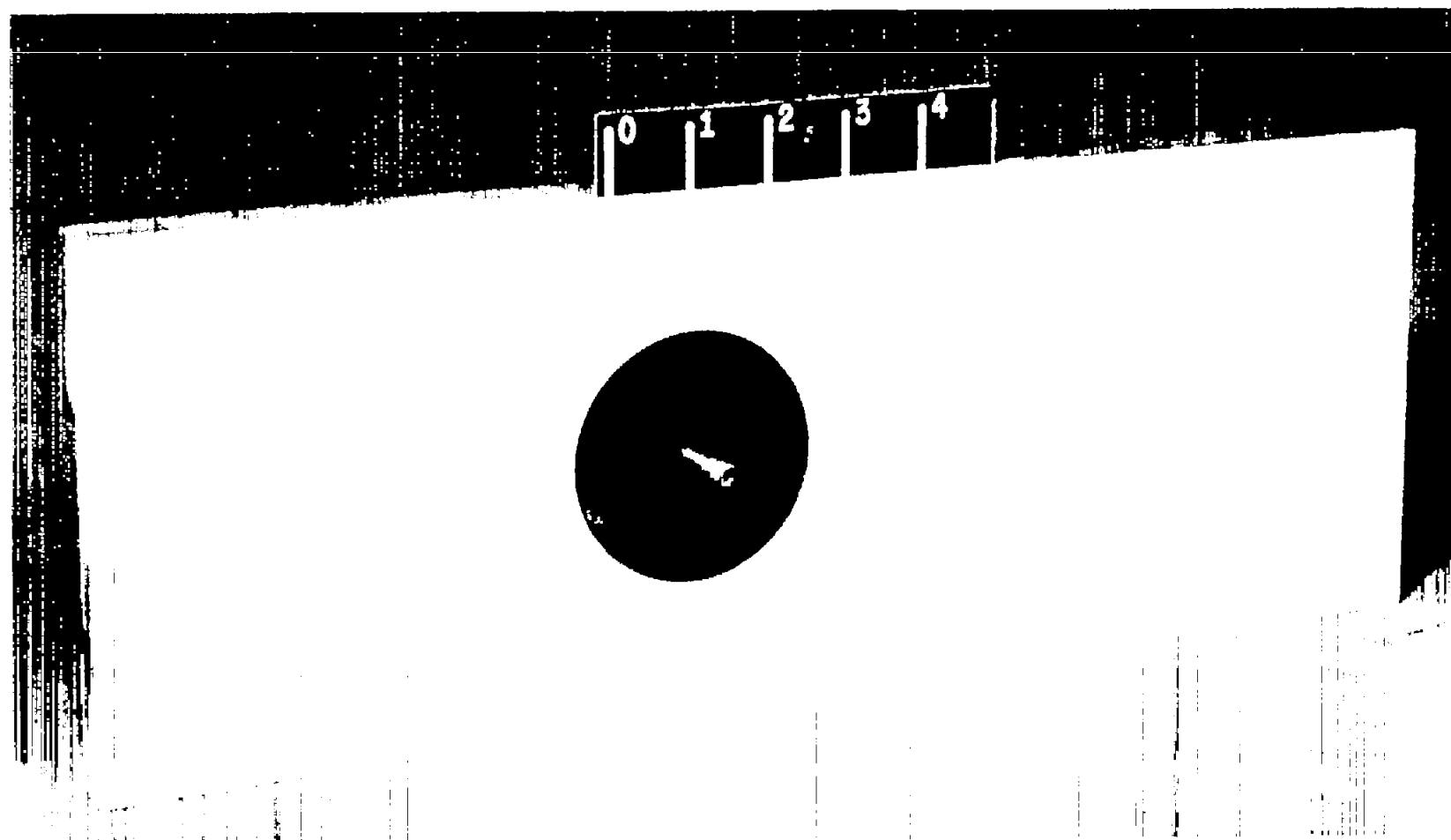
	1.0	0	Good			12(a)	—	9(a)
	0.87	30	Good			12(b)	—	9(b)

NACA TN 3559



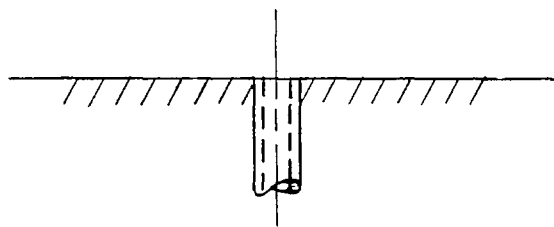
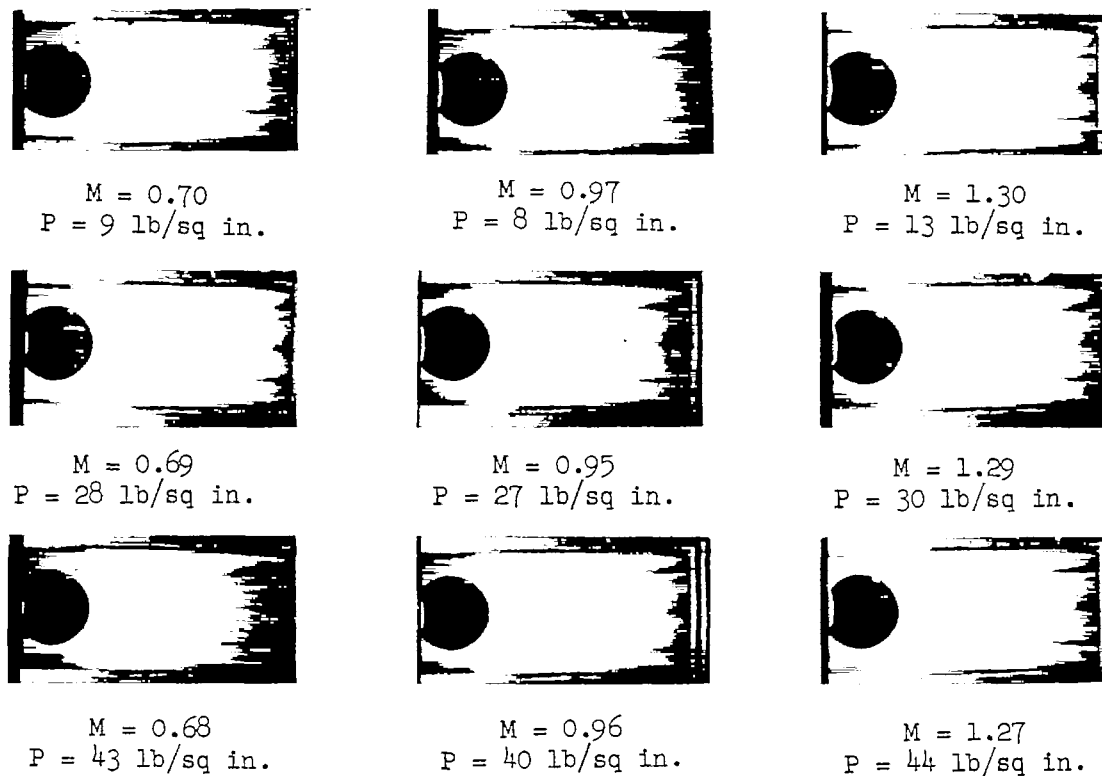
L-82977

Figure 1.- Photograph of the $4\frac{1}{2}$ -by $6\frac{1}{4}$ -inch tunnel used for schlieren pictures and drag measurements.



L-83261

Figure 2.- Photograph of the side plate for the $4\frac{1}{2}$ -by $4\frac{1}{2}$ -inch tunnel
used for stain pictures.

(a) $\Lambda = 0^\circ$; flush drain.

L-85595

Figure 3.- Stain patterns produced by liquid flowing from various drains for a constant interval of 30 seconds.



$M = 0.68$
 $P = 6 \text{ lb/sq in.}$



$M = 0.99$
 $P = 8 \text{ lb/sq in.}$



$M = 1.32$
 $P = 11 \text{ lb/sq in.}$



$M = 0.68$
 $P = 25 \text{ lb/sq in.}$



$M = 0.97$
 $P = 23 \text{ lb/sq in.}$



$M = 1.29$
 $P = 29 \text{ lb/sq in.}$



$M = 0.67$
 $P = 42 \text{ lb/sq in.}$



$M = 0.97$
 $P = 40 \text{ lb/sq in.}$



$M = 1.28$
 $P = 43 \text{ lb/sq in.}$

(b) $\Lambda = 0^\circ$; 1-inch extension.



$M = 0.68$
 $P = 6 \text{ lb/sq in.}$



$M = 0.99$
 $P = 1 \text{ lb/sq in.}$



$M = 1.31$
 $P = 12 \text{ lb/sq in.}$



$M = 0.68$
 $P = 25 \text{ lb/sq in.}$



$M = 1.00$
 $P = 22 \text{ lb/sq in.}$



$M = 1.31$
 $P = 26 \text{ lb/sq in.}$



$M = 0.68$
 $P = 40 \text{ lb/sq in.}$



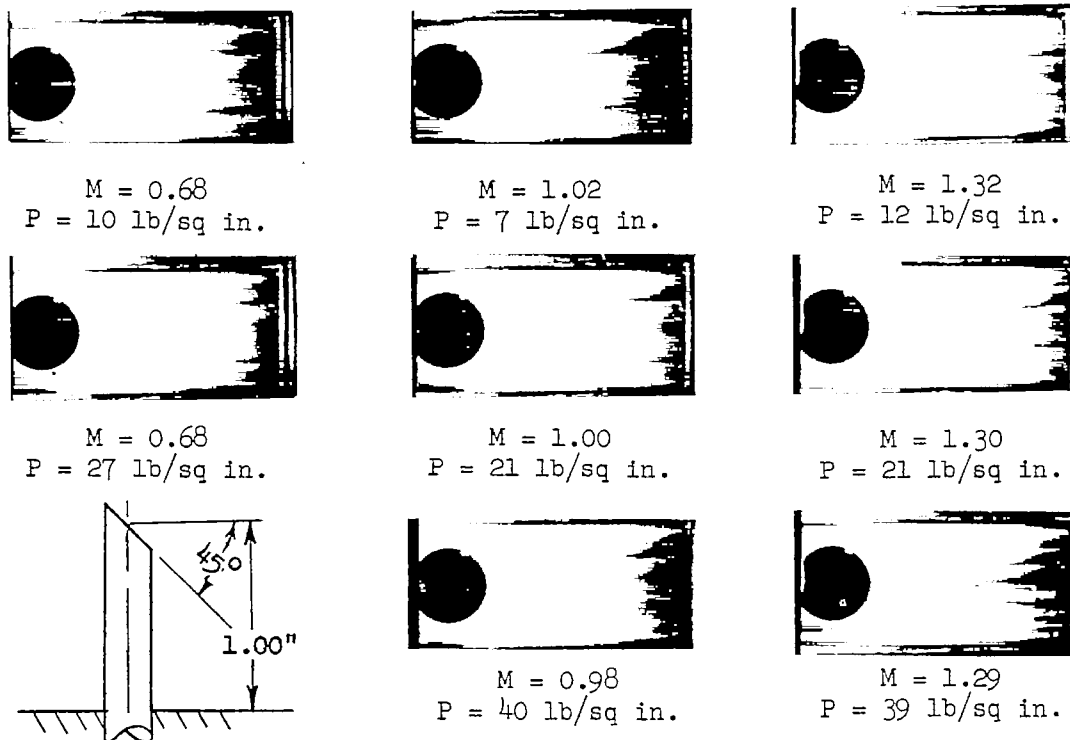
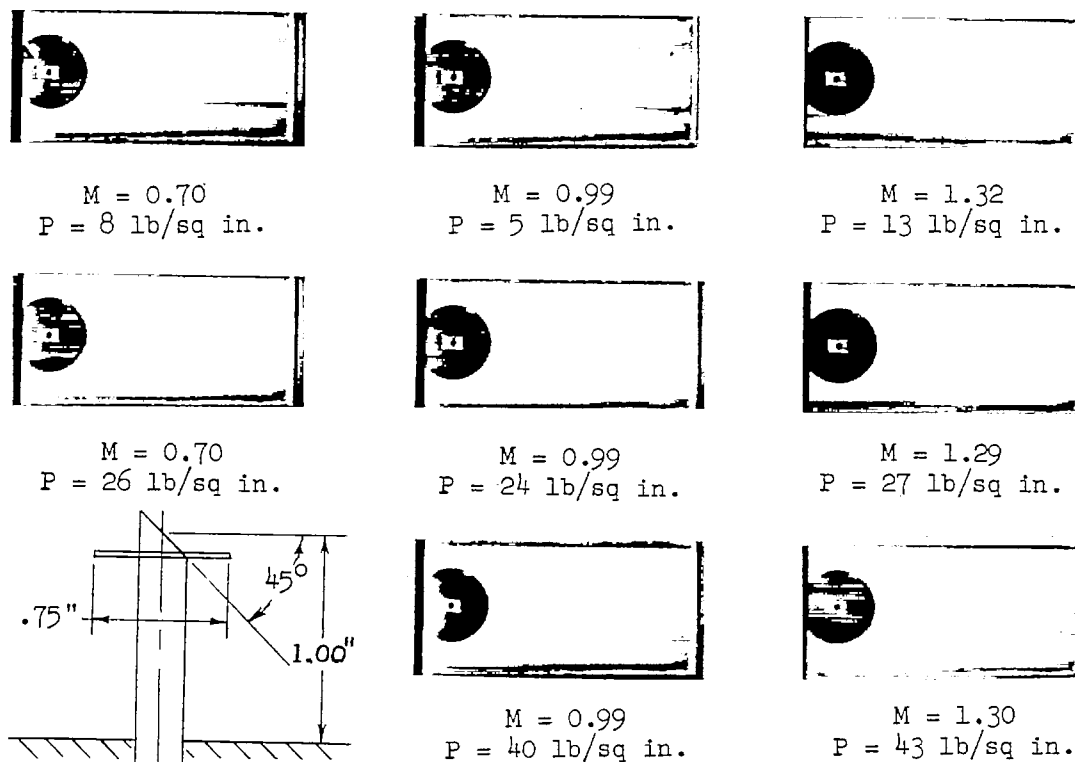
$M = 0.94$
 $P = 38 \text{ lb/sq in.}$



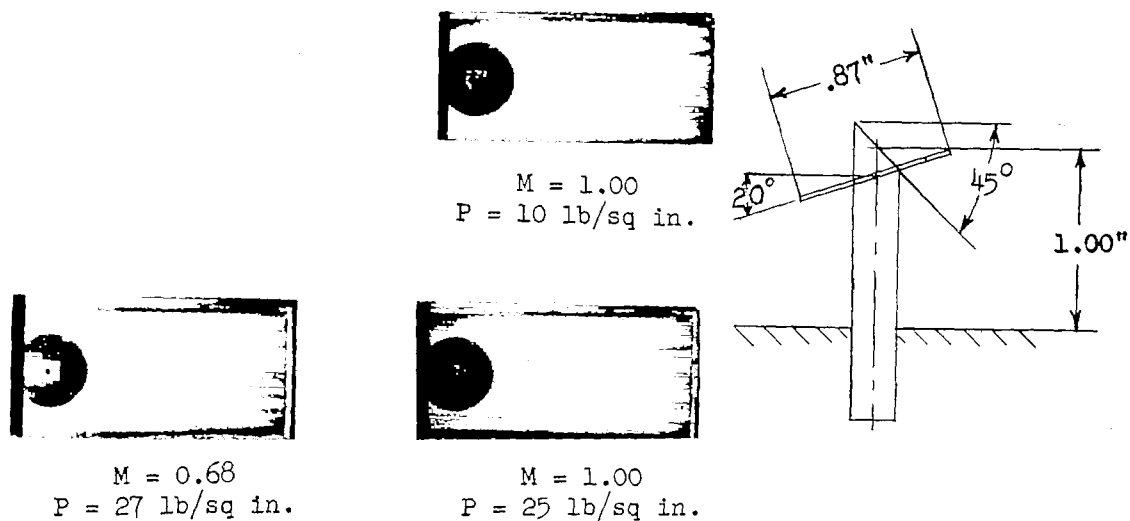
$M = 1.31$
 $P = 42 \text{ lb/sq in.}$

(c) $\Lambda = 0^\circ$; 2-inch extension.

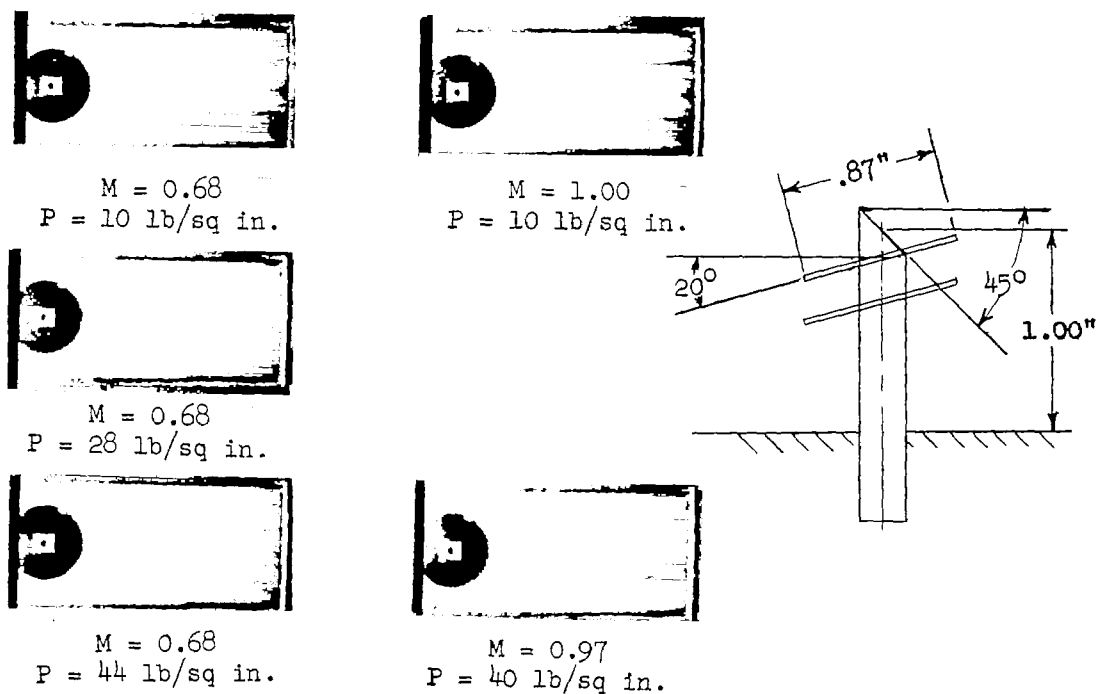
L-85596

(d) $\Lambda = 0^\circ$; 1-inch extension; 45° chamfer.(e) $\Lambda = 0^\circ$; 1-inch extension; 45° chamfer; 1 vane at 0° angle of attack.

L-85597



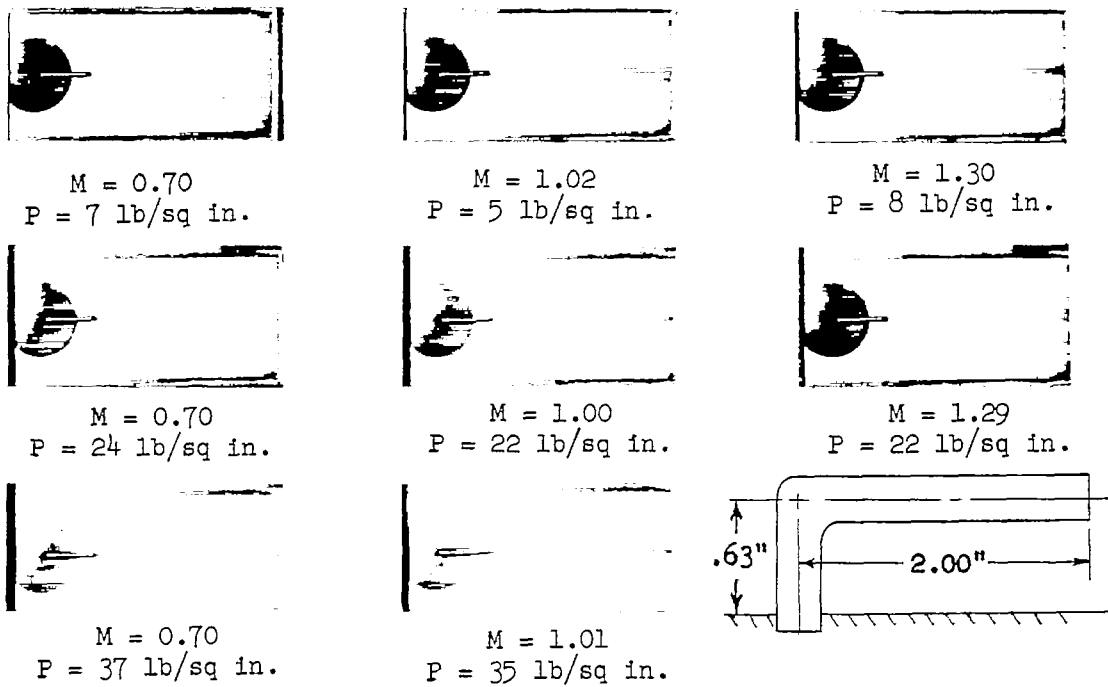
(f) $\Lambda = 0^\circ$; 1-inch extension; 45° chamfer; 1 vane at -20° angle of attack.



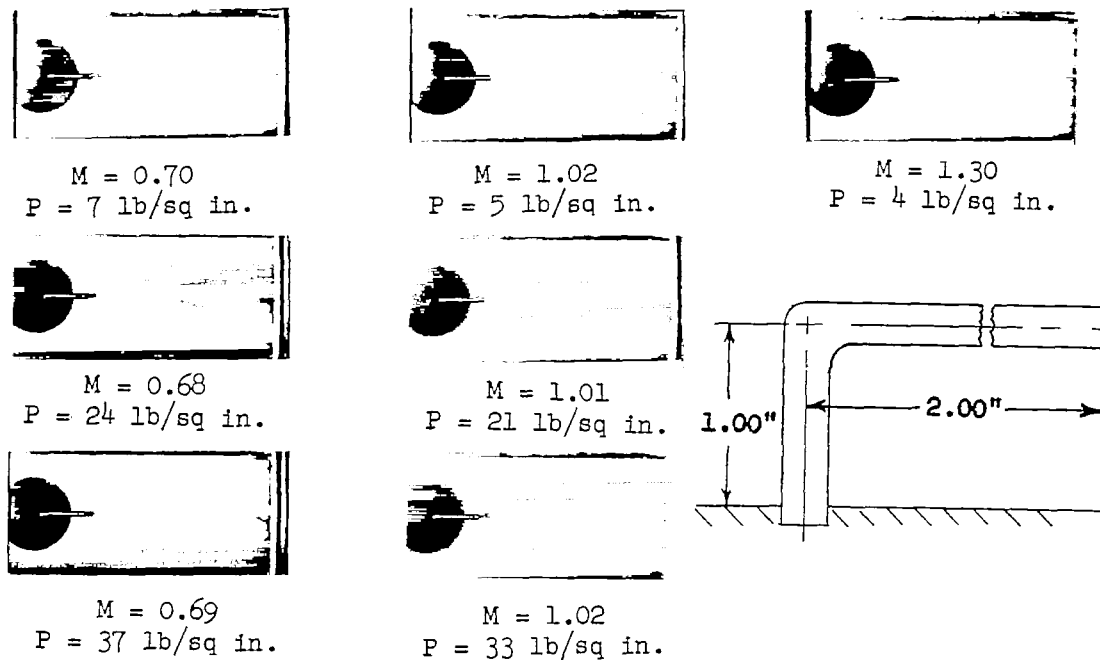
(g) $\Lambda = 0^\circ$; 1-inch extension; 45° chamfer; 2 vanes at -20° angle of attack.

L-85598

Figure 3.- Continued.



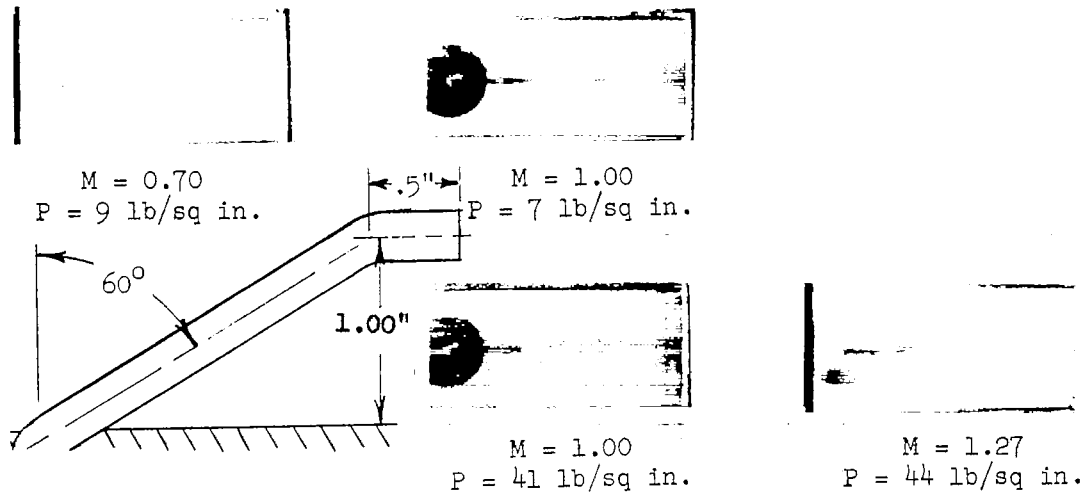
(h) $\Lambda = 0^\circ$; 5/8-inch extension; 90° bend; 2-inch straight section.



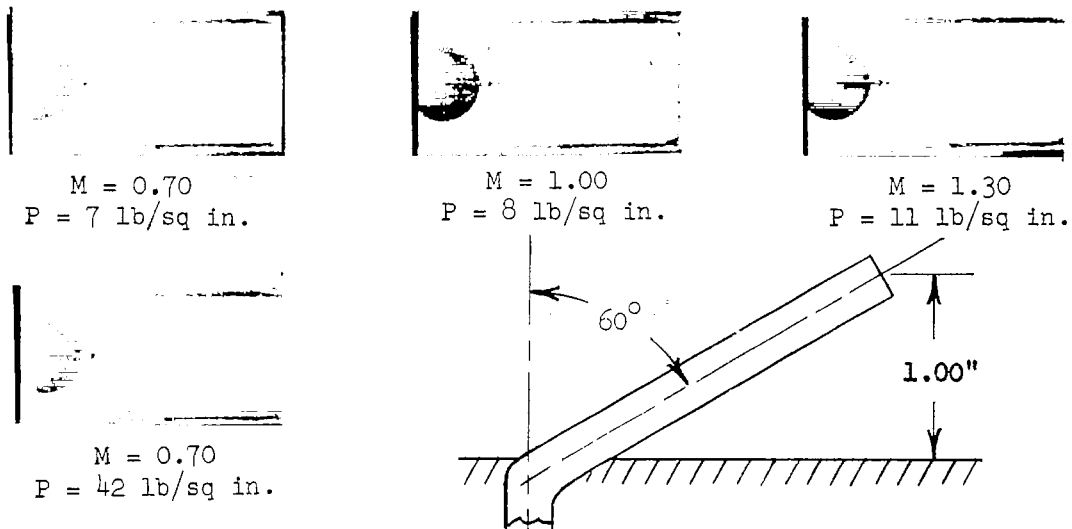
(i) $\Lambda = 0^\circ$; 1-inch extension; 90° bend; 2-inch straight section.

L-85599

Figure 3.- Continued.



(j) $\Lambda = 60^\circ$; 1-inch extension (projected); 30° bend;
 1/2-inch straight section.



(k) $\Lambda = 60^\circ$; 1-inch extension (projected). L-85600

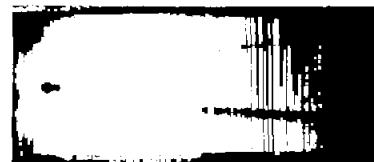
Figure 3.- Concluded.



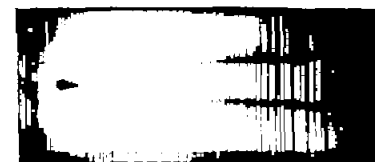
$M = 0.50$
 $\Delta p = 2.2 \text{ lb/sq in.}$
 $P = 40 \text{ lb/sq in.}$



$M = 0.70$
 $\Delta p = 4.6 \text{ lb/sq in.}$
 $P = 41 \text{ lb/sq in.}$



$M = 1.01$
 $\Delta p = 12.7 \text{ lb/sq in.}$
 $P = 39 \text{ lb/sq in.}$



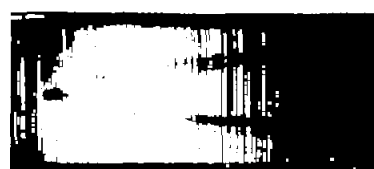
$M = 1.29$
 $\Delta p = 17.2 \text{ lb/sq in.}$
 $P = 39 \text{ lb/sq in.}$



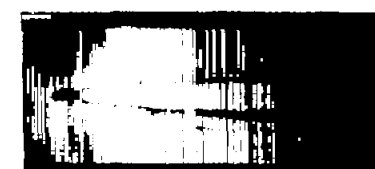
$M = 0.50$
 $\Delta p = 2.3 \text{ lb/sq in.}$
 $P = 5 \text{ lb/sq in.}$



$M = 0.70$
 $\Delta p = 4.6 \text{ lb/sq in.}$
 $P = 6 \text{ lb/sq in.}$



$M = 1.02$
 $\Delta p = 12.9 \text{ lb/sq in.}$
 $P = 15 \text{ lb/sq in.}$



$M = 1.29$
 $\Delta p = 17.4 \text{ lb/sq in.}$
 $P = 17 \text{ lb/sq in.}$



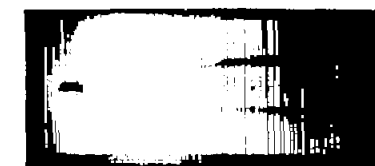
$M = 0.50$
 $\Delta p = 0.5 \text{ lb/sq in.}$
 $P = 40 \text{ lb/sq in.}$



$M = 0.70$
 $\Delta p = 1.1 \text{ lb/sq in.}$
 $P = 41 \text{ lb/sq in.}$



$M = 1.01$
 $\Delta p = 5.5 \text{ lb/sq in.}$
 $P = 39 \text{ lb/sq in.}$

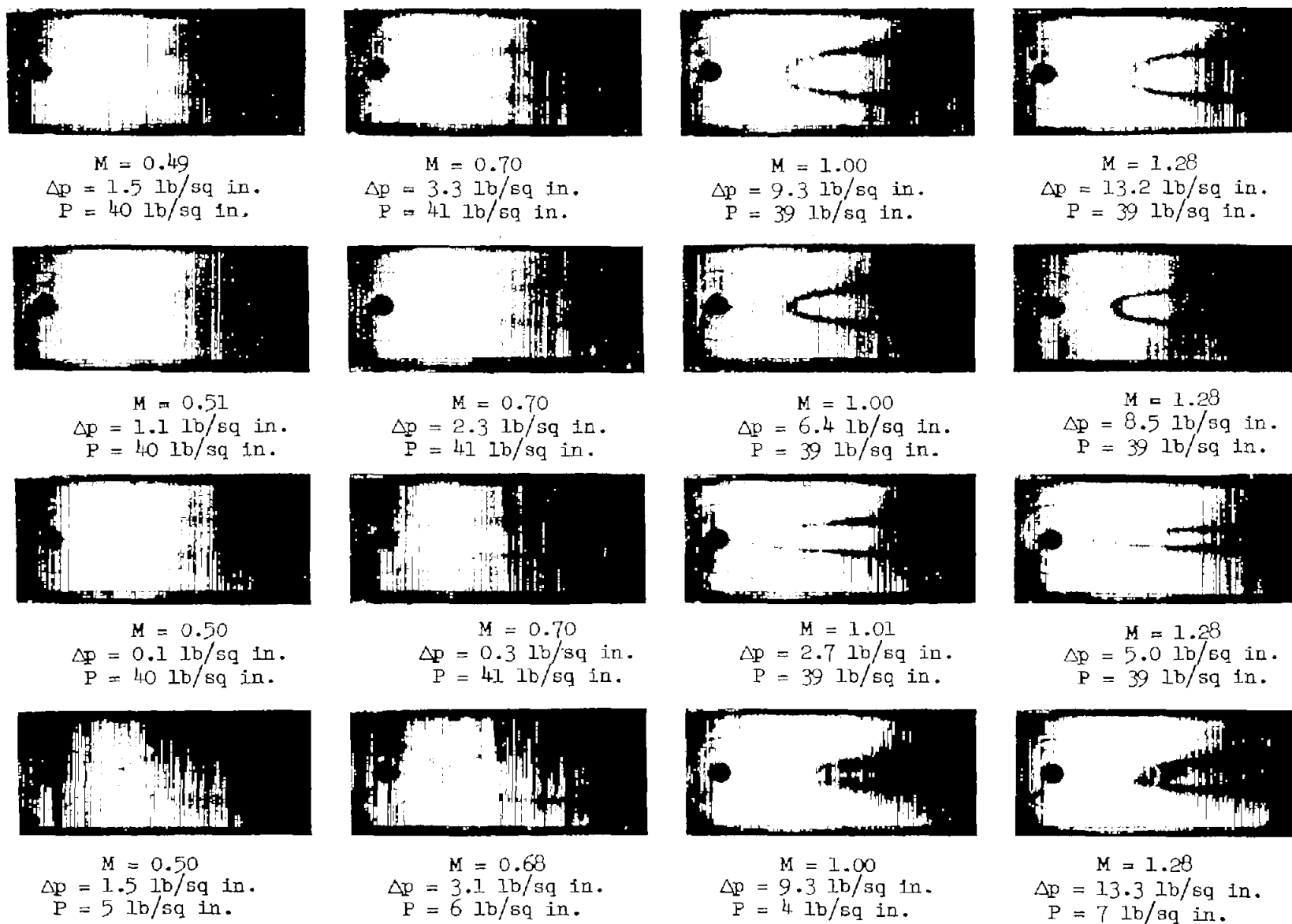


$M = 1.29$
 $\Delta p = 10.3 \text{ lb/sq in.}$
 $P = 39 \text{ lb/sq in.}$

(a) $\Lambda = 0^\circ$; 3/8-inch-diameter outlet; 1-inch extension.

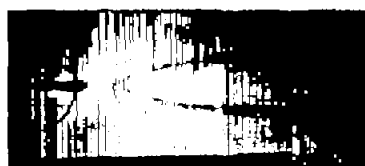
L-85601

Figure 4.- Stain patterns produced by liquid flowing from 1/4-inch drains inserted in air outlets.

(b) $\Lambda = 0^\circ$; 7/8-inch-diameter outlet; 1-inch extension.

L-85602

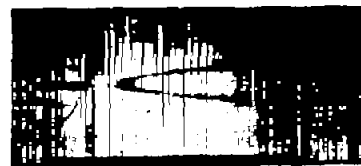
Figure 4.- Continued.



$M = 0.50$
 $\Delta p = 2.2 \text{ lb/sq in.}$
 $P = 40 \text{ lb/sq in.}$



$M = 0.70$
 $\Delta p = 4.3 \text{ lb/sq in.}$
 $P = 41 \text{ lb/sq in.}$



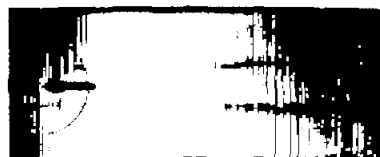
$M = 1.01$
 $\Delta p = 11.6 \text{ lb/sq in.}$
 $P = 39 \text{ lb/sq in.}$



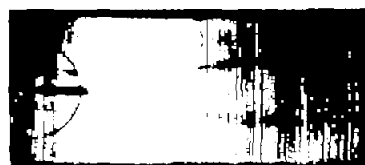
$M = 1.30$
 $\Delta p = 15.7 \text{ lb/sq in.}$
 $P = 39 \text{ lb/sq in.}$



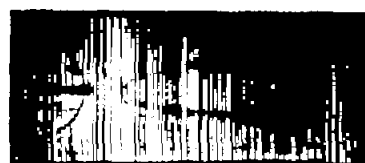
$M = 0.50$
 $\Delta p = 1.0 \text{ lb/sq in.}$
 $P = 40 \text{ lb/sq in.}$



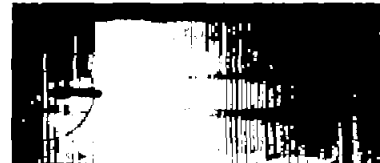
$M = 0.70$
 $\Delta p = 2.1 \text{ lb/sq in.}$
 $P = 41 \text{ lb/sq in.}$



$M = 0.50$
 $\Delta p = 0.2 \text{ lb/sq in.}$
 $P = 40 \text{ lb/sq in.}$



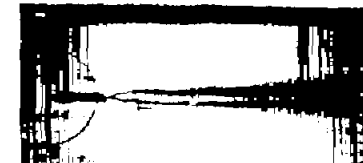
$M = 0.50$
 $\Delta p = 2.1 \text{ lb/sq in.}$
 $P = 5 \text{ lb/sq in.}$



$M = 0.70$
 $\Delta p = 4.3 \text{ lb/sq in.}$
 $P = 6 \text{ lb/sq in.}$



$M = 1.01$
 $\Delta p = 11.6 \text{ lb/sq in.}$
 $P = 4 \text{ lb/sq in.}$



$M = 1.30$
 $\Delta p = 15.8 \text{ lb/sq in.}$
 $P = 7 \text{ lb/sq in.}$

(c) $\Lambda = 60^\circ$; 3/8-inch-diameter outlet; 1/2-inch extension (projected).

L-85603

Figure 4.- Concluded.

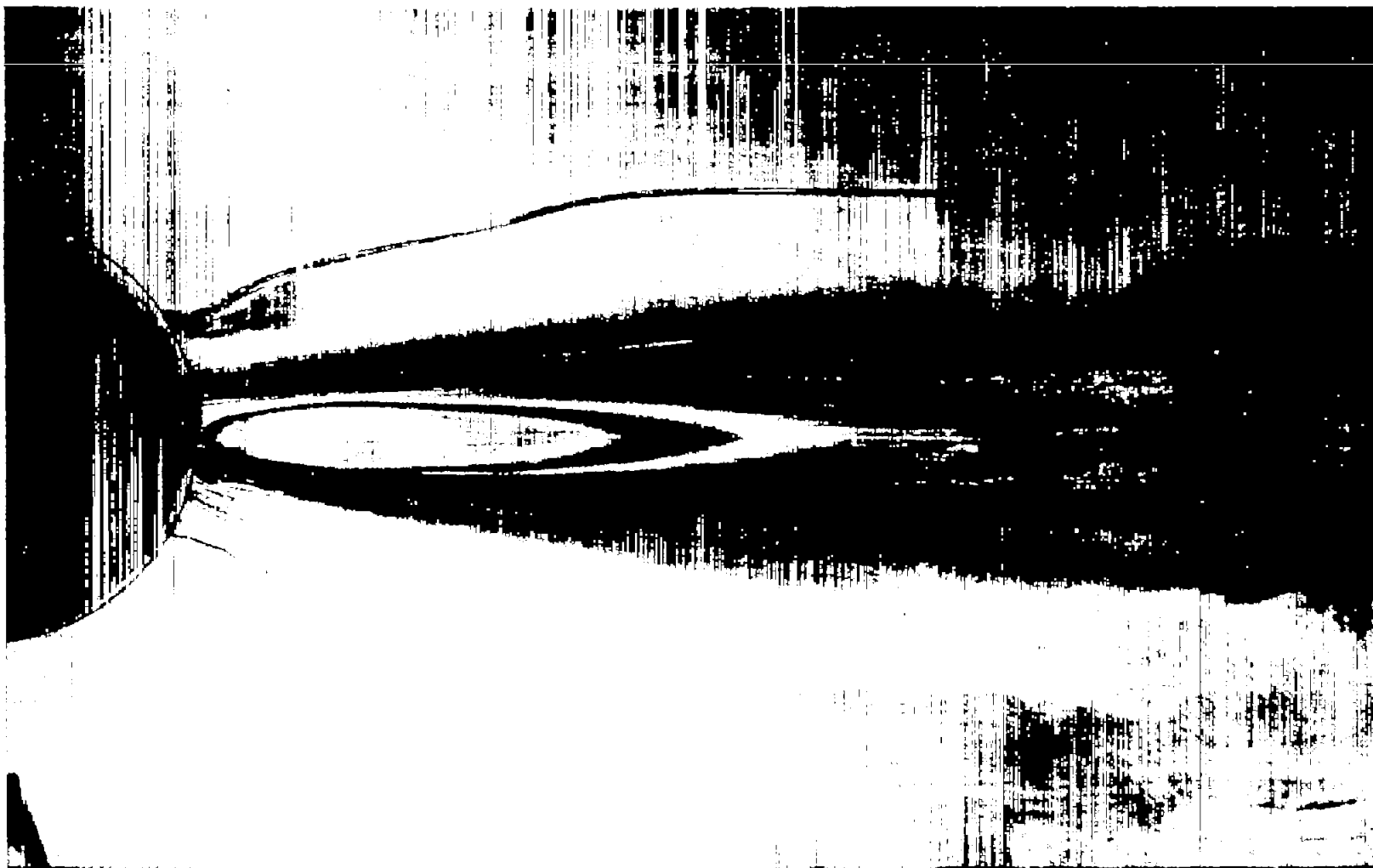
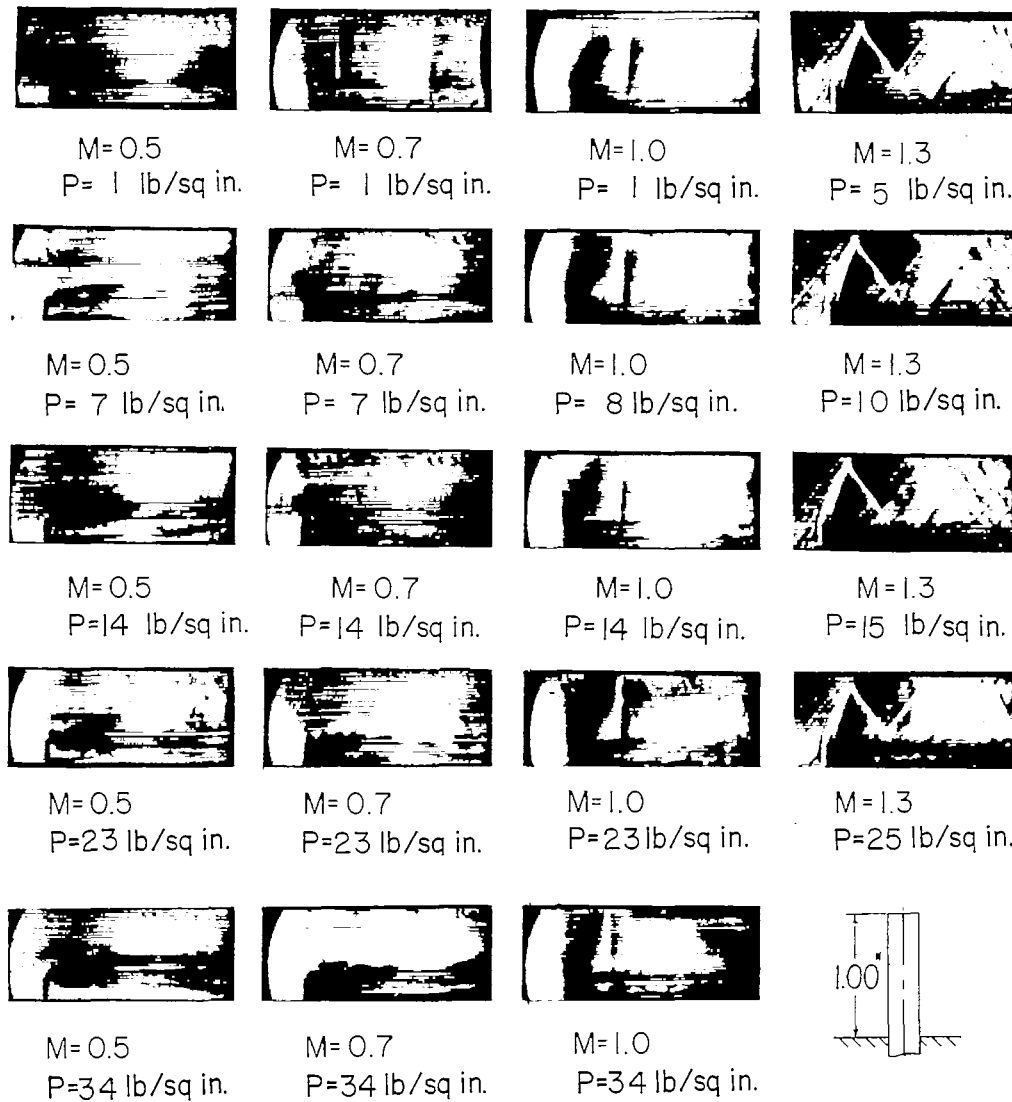


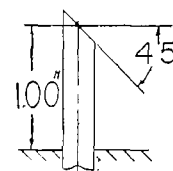
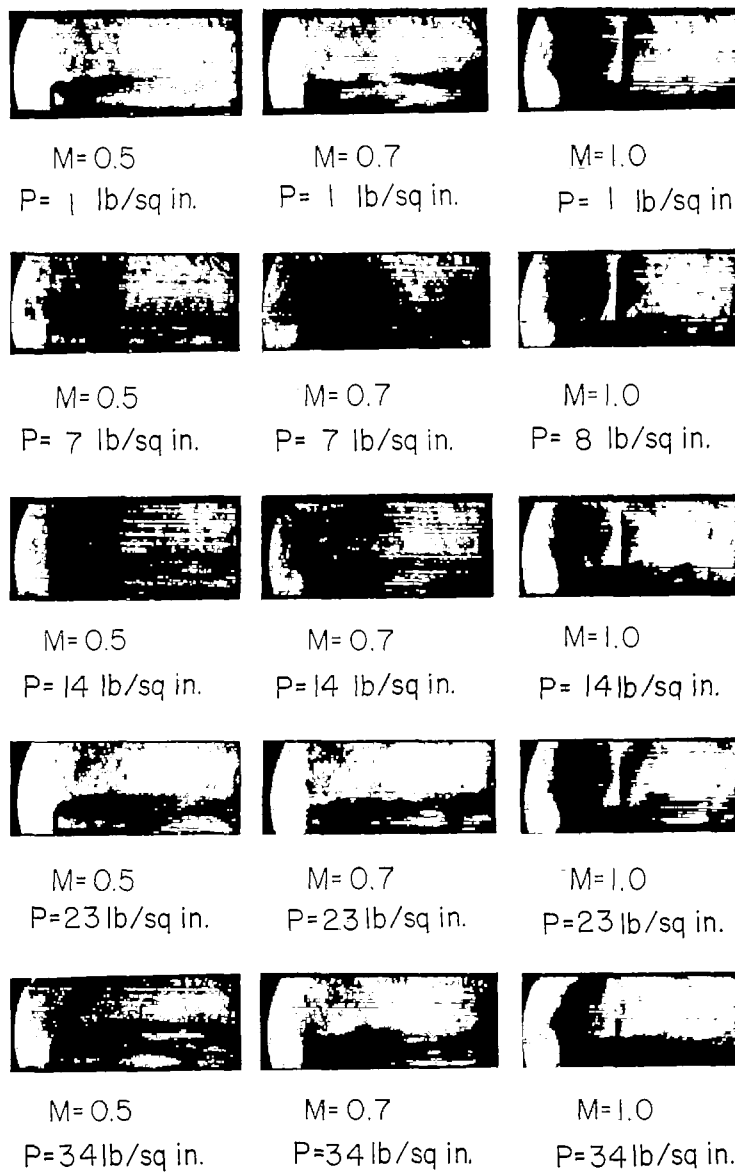
Figure 5.- Surface staining at low flow rates (dripping). $M = 1.2$; $\Lambda = 0^\circ$; 1-inch extension. L-85604



(a) $\Lambda = 0^\circ$; 1-inch extension.

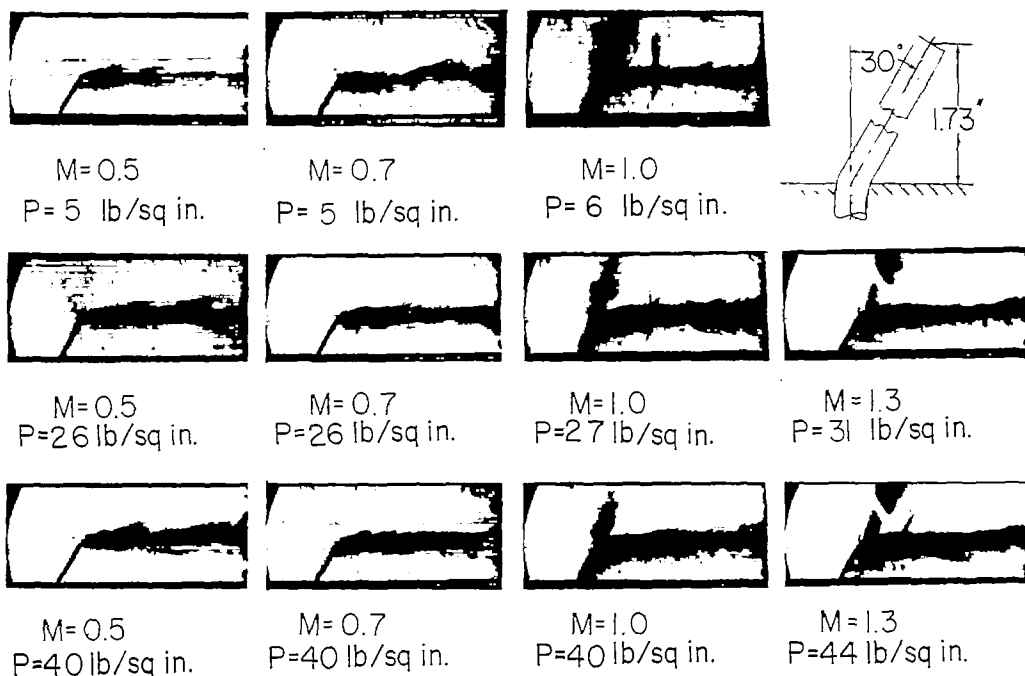
L-85605

Figure 6.- Schlieren photographs of liquid flowing from various cylindrical drains.

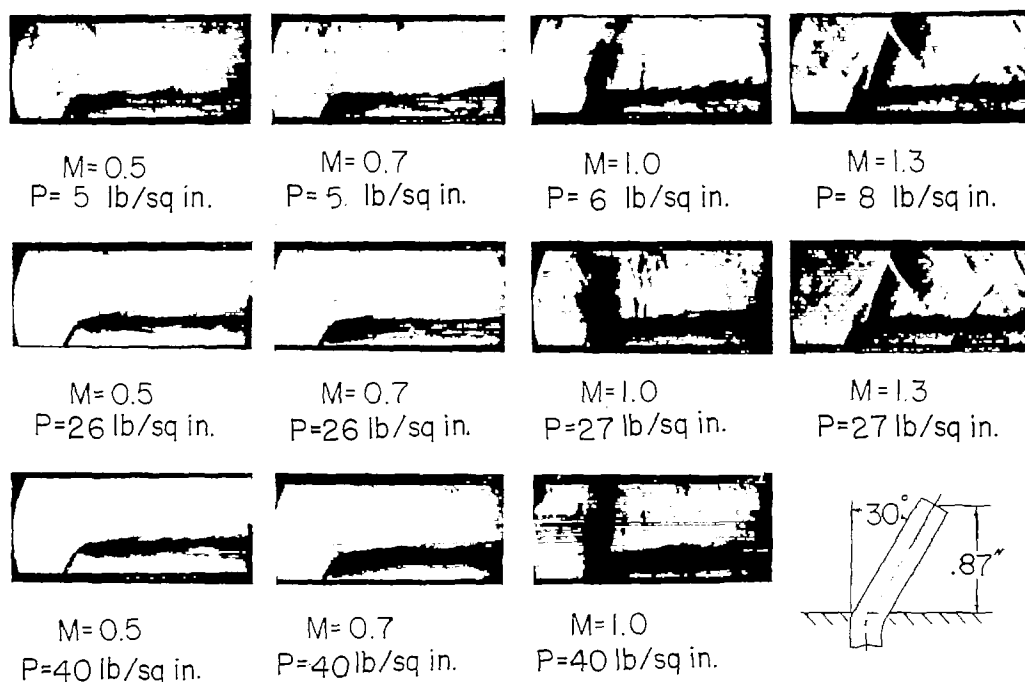


(b) $\Lambda = 0^\circ$; 1-inch extension; 45° chamfer. L-85606

Figure 6.- Continued.

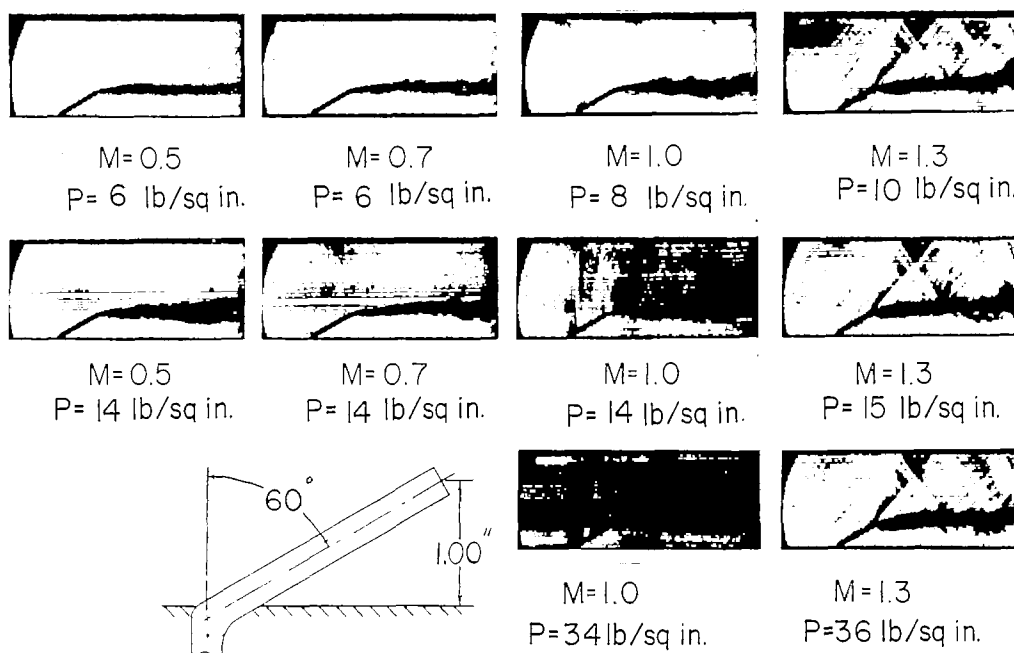


(c) $\Lambda = 30^\circ$; 1.73-inch extension (projected).

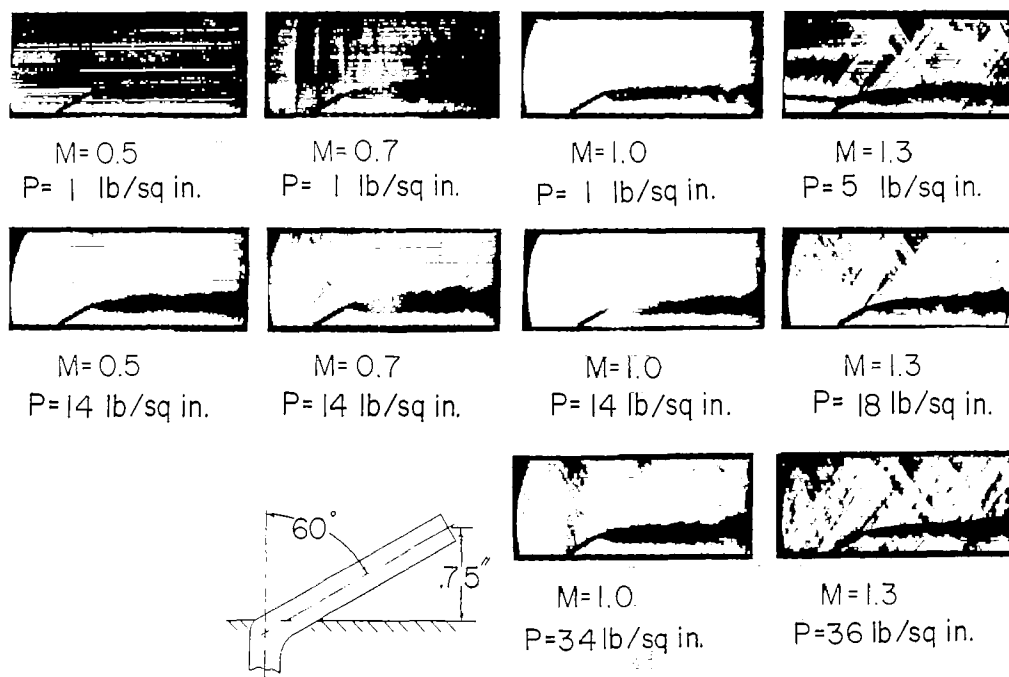


(d) $\Lambda = 30^\circ$; 0.87-inch extension (projected). L-85607

Figure 6.- Continued.

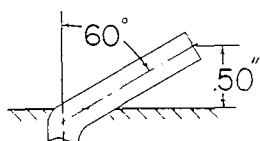
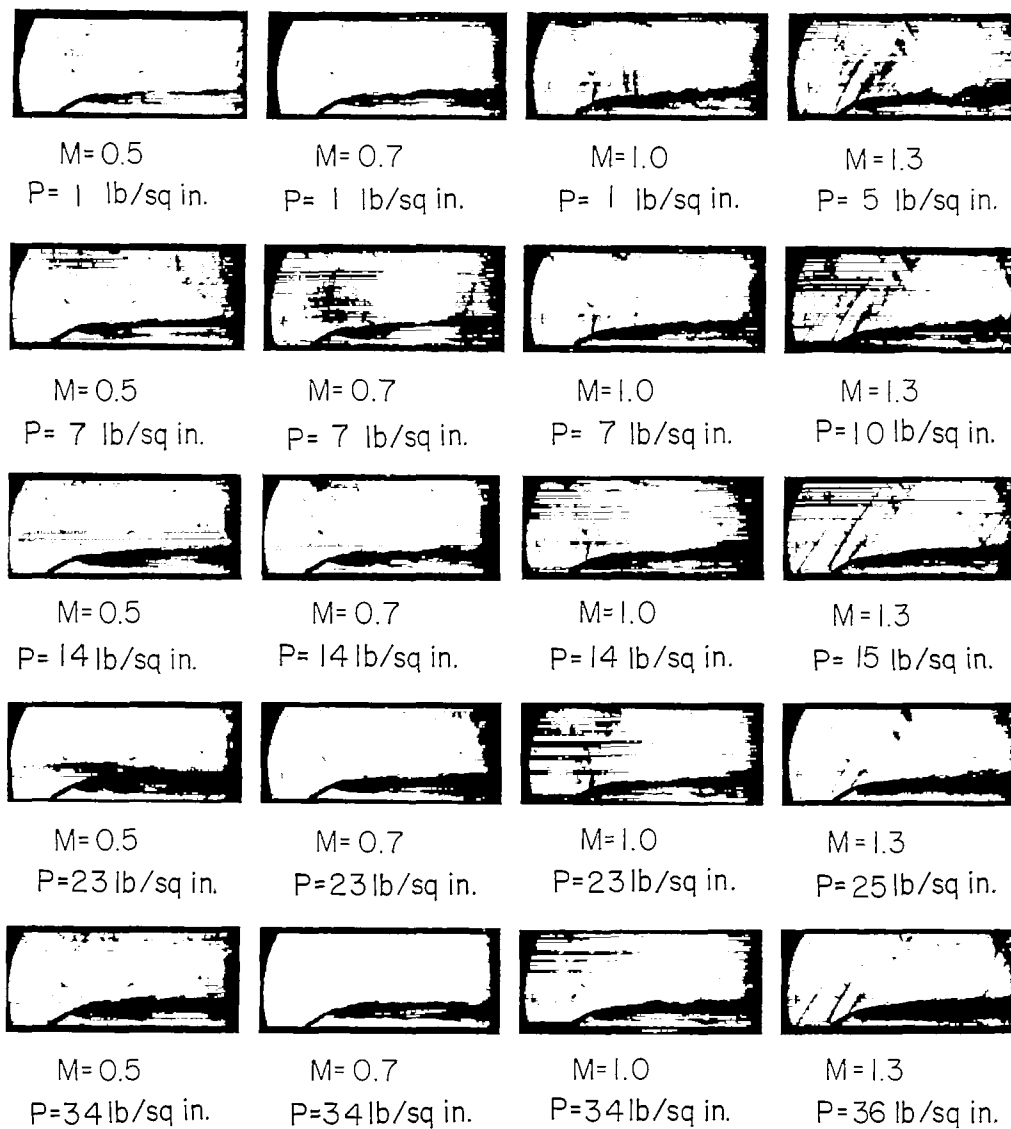


(e) $\Lambda = 60^\circ$; 1-inch extension (projected).



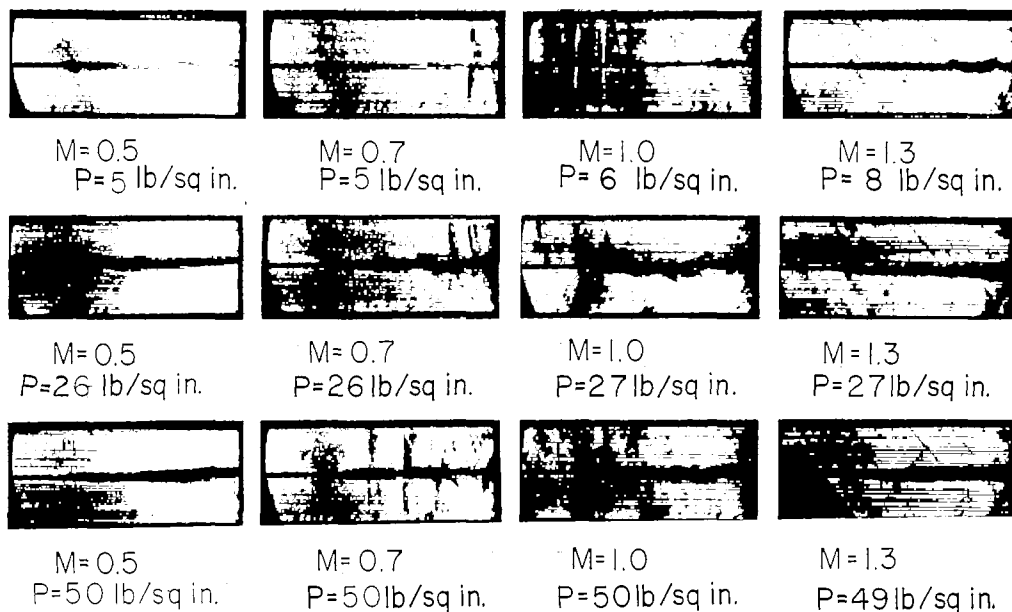
(f) $\Lambda = 60^\circ$; 0.75-inch extension (projected).

L-85608

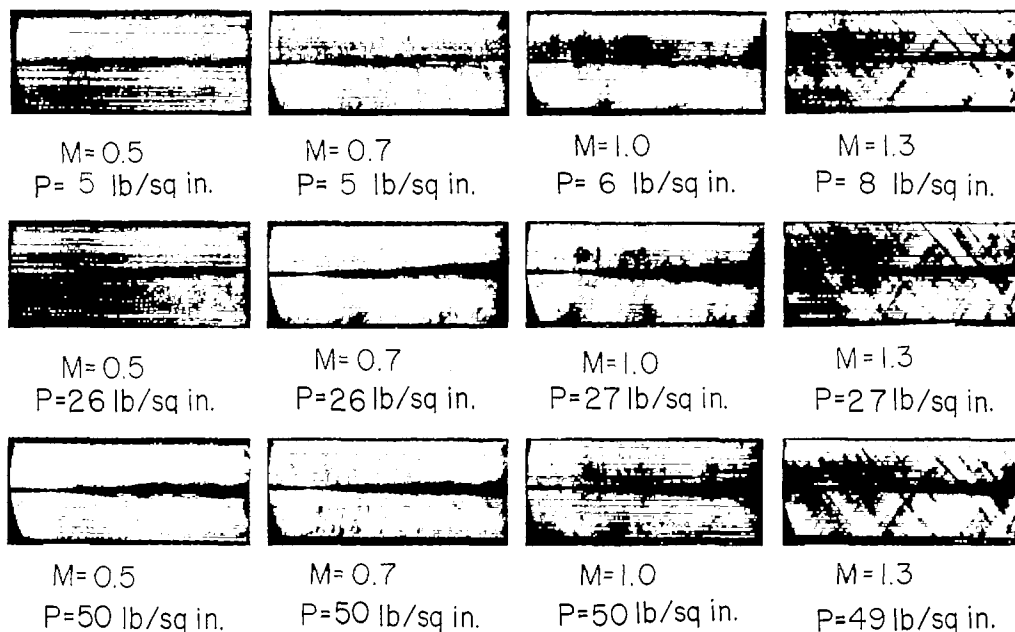


(g) $\Delta = 60^\circ$; 0.50-inch extension (projected). L-85609

Figure 6.- Concluded.

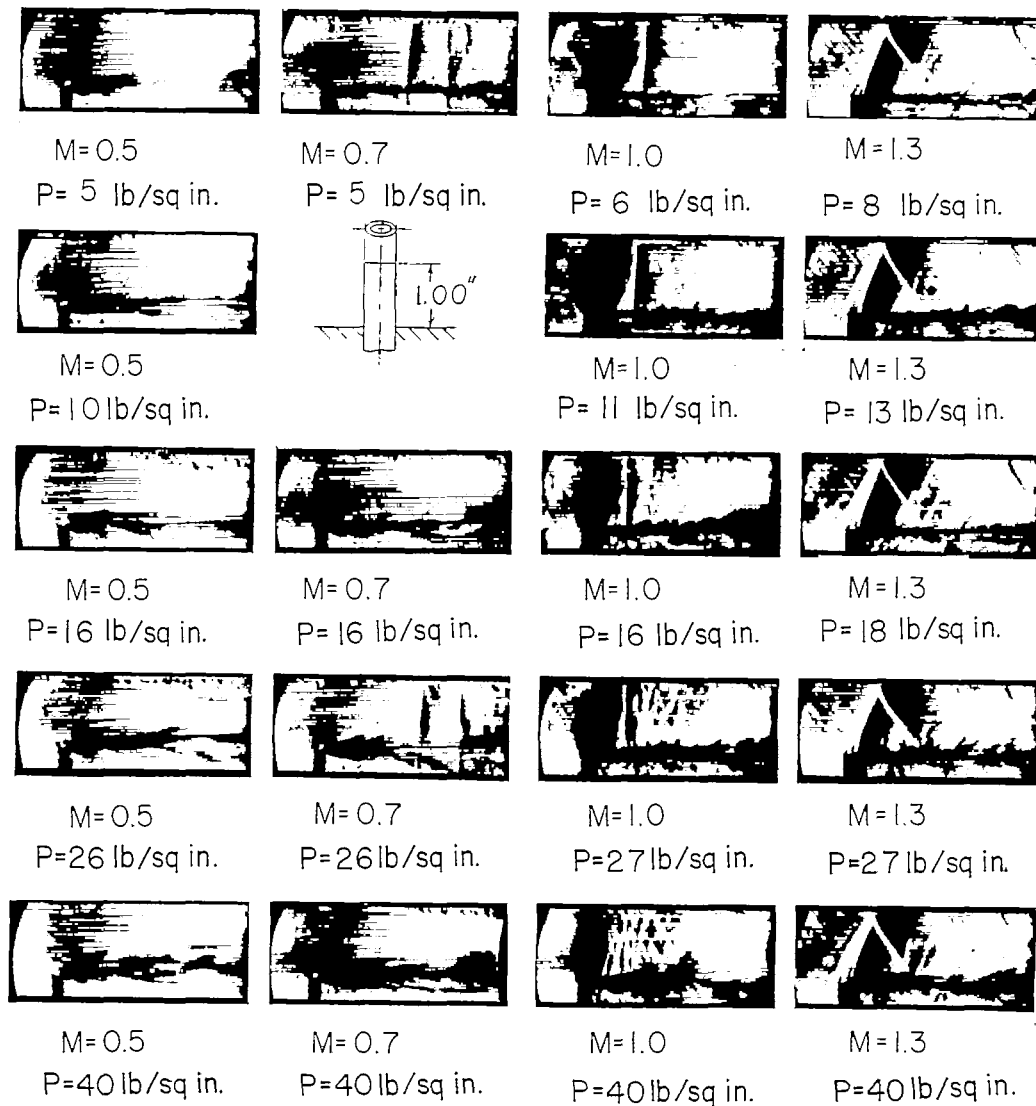


(a) 1/4-inch O.D. by 1/8-inch I.D. drain with no end taper.



(b) 1/4-inch O.D. by 1/8-inch I.D. drain with end tapered for a distance of 1.25 inch.

Figure 7.- Schlieren photographs of liquid flowing from drain parallel with airstream.

(a) $\Lambda = 0^\circ$; 1-inch extension.

L-85611

Figure 8.- Schlieren photographs of liquid flowing from elliptical drains.

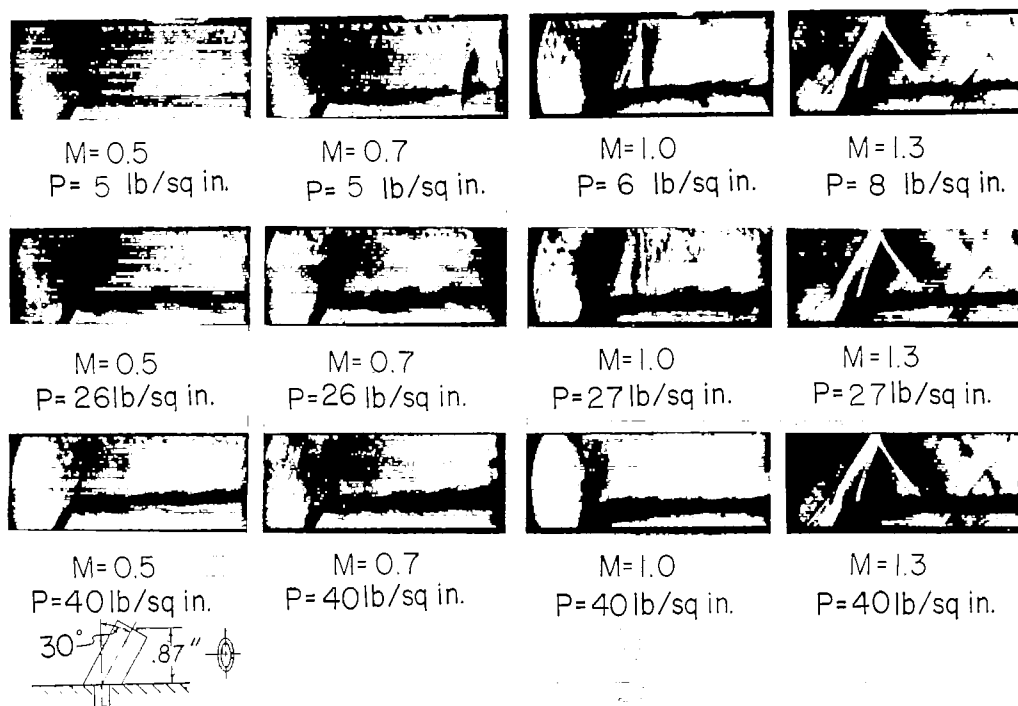
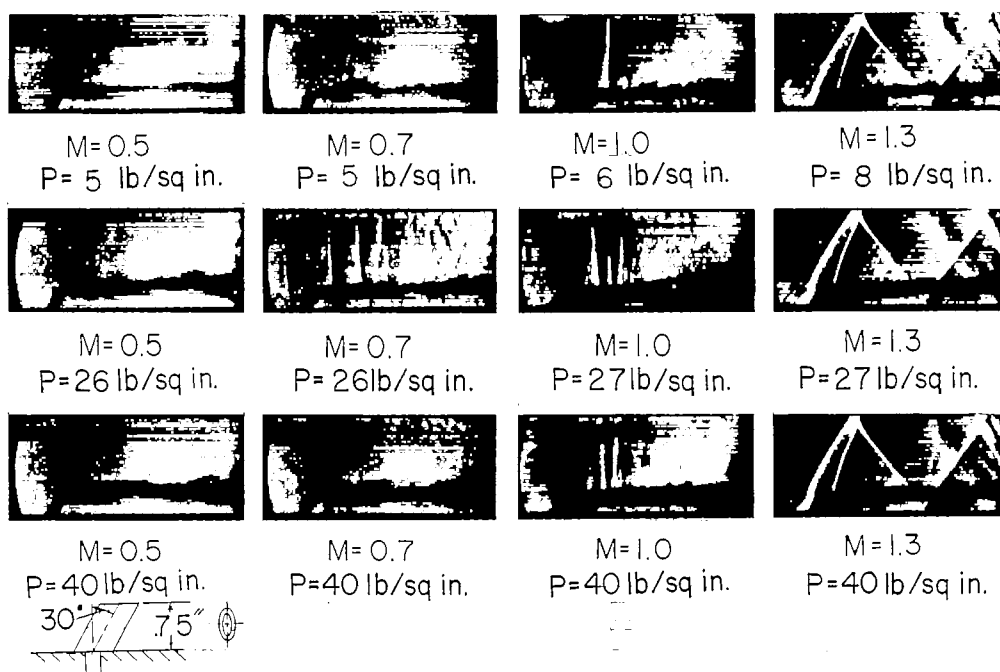
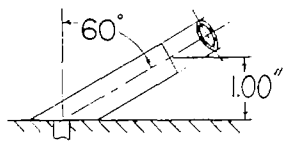
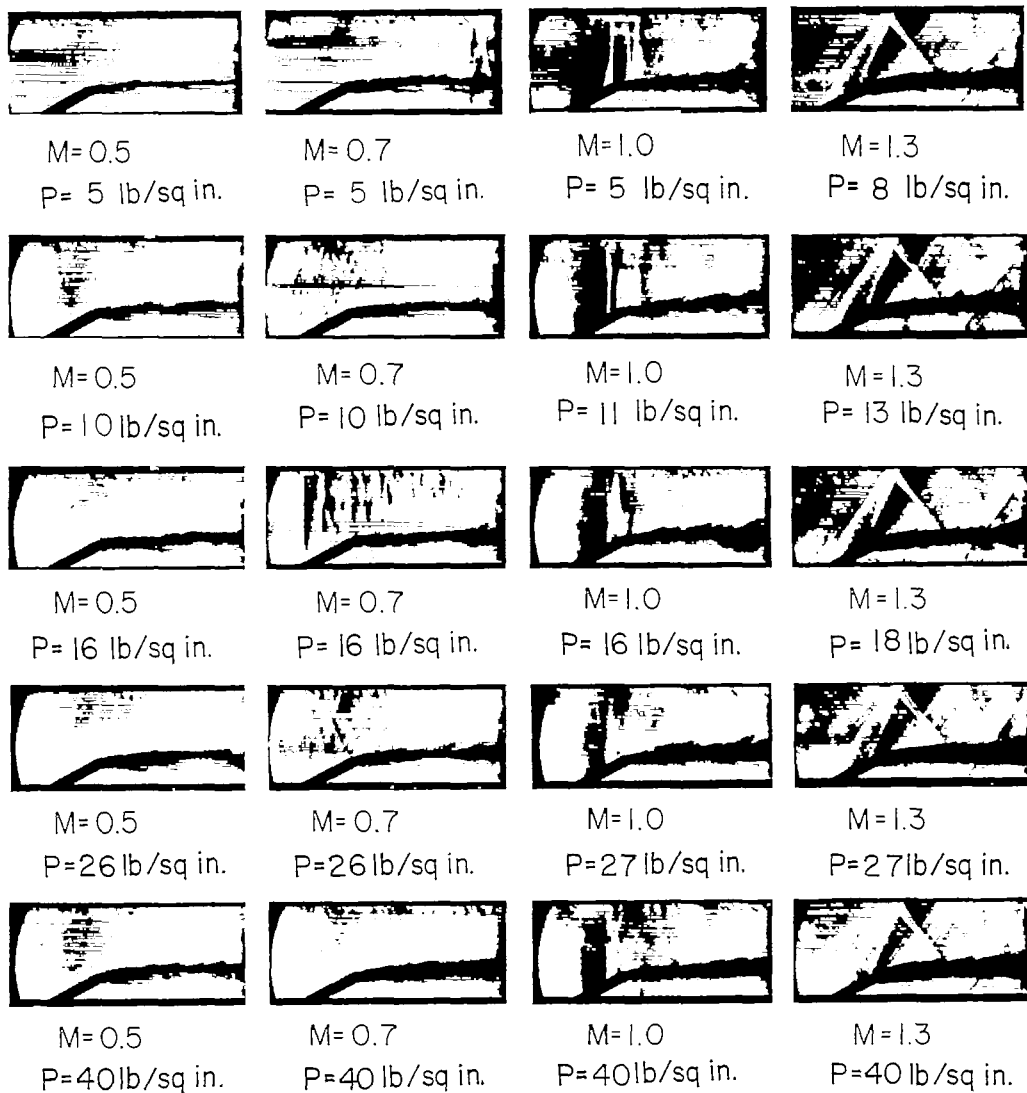
(b) $\Lambda = 30^\circ$; 0.87-inch extension (projected).(c) $\Lambda = 30^\circ$; 0.75-inch extension (projected); end of drain cut parallel with airstream. L-85612

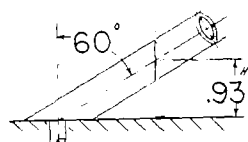
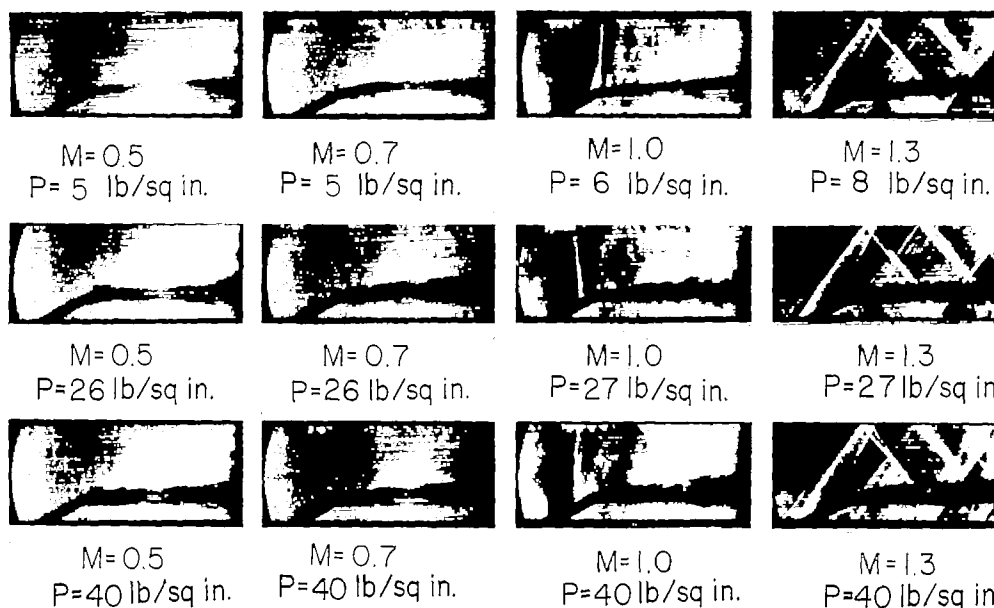
Figure 8.- Continued.



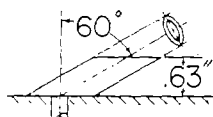
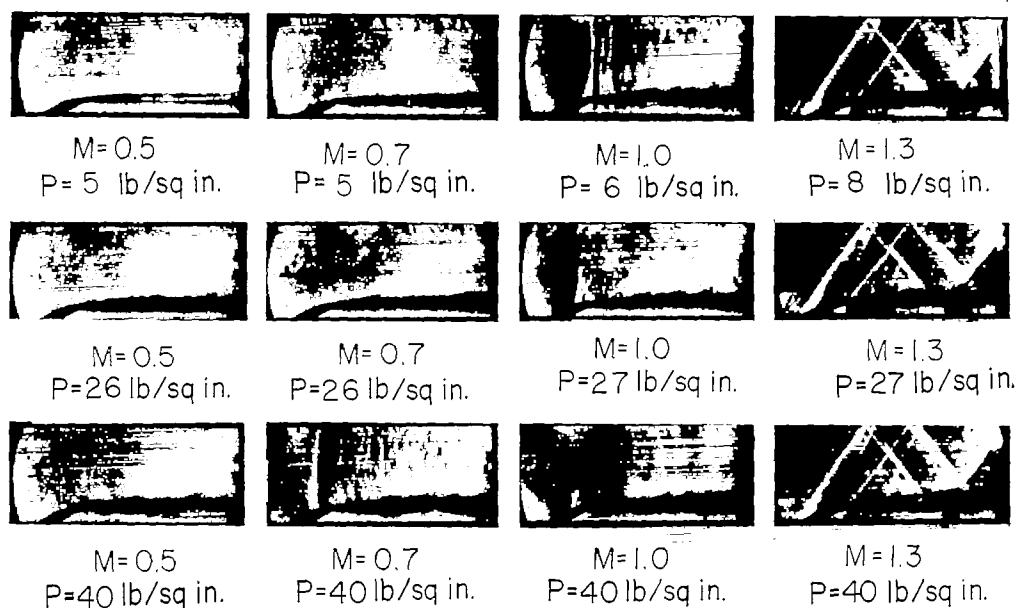
(d) $\Lambda = 60^\circ$; 1-inch extension (projected).

L-85613

Figure 8.- Continued.



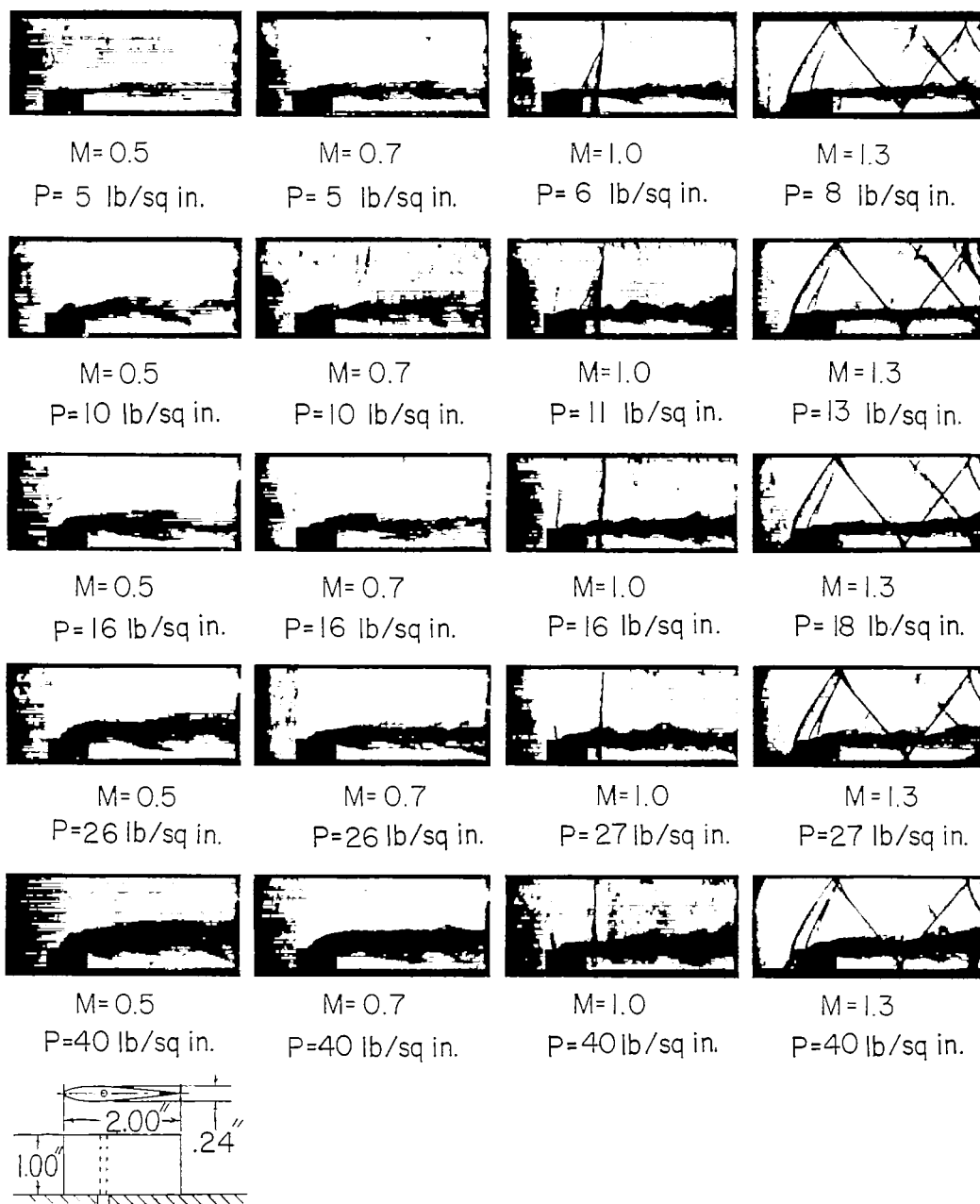
(e) $\Lambda = 60^\circ$; 0.93-inch extension (projected);
end of drain cut normal to airstream.



(f) $\Lambda = 60^\circ$; 0.63-inch extension (projected);
end of drain cut parallel with airstream.

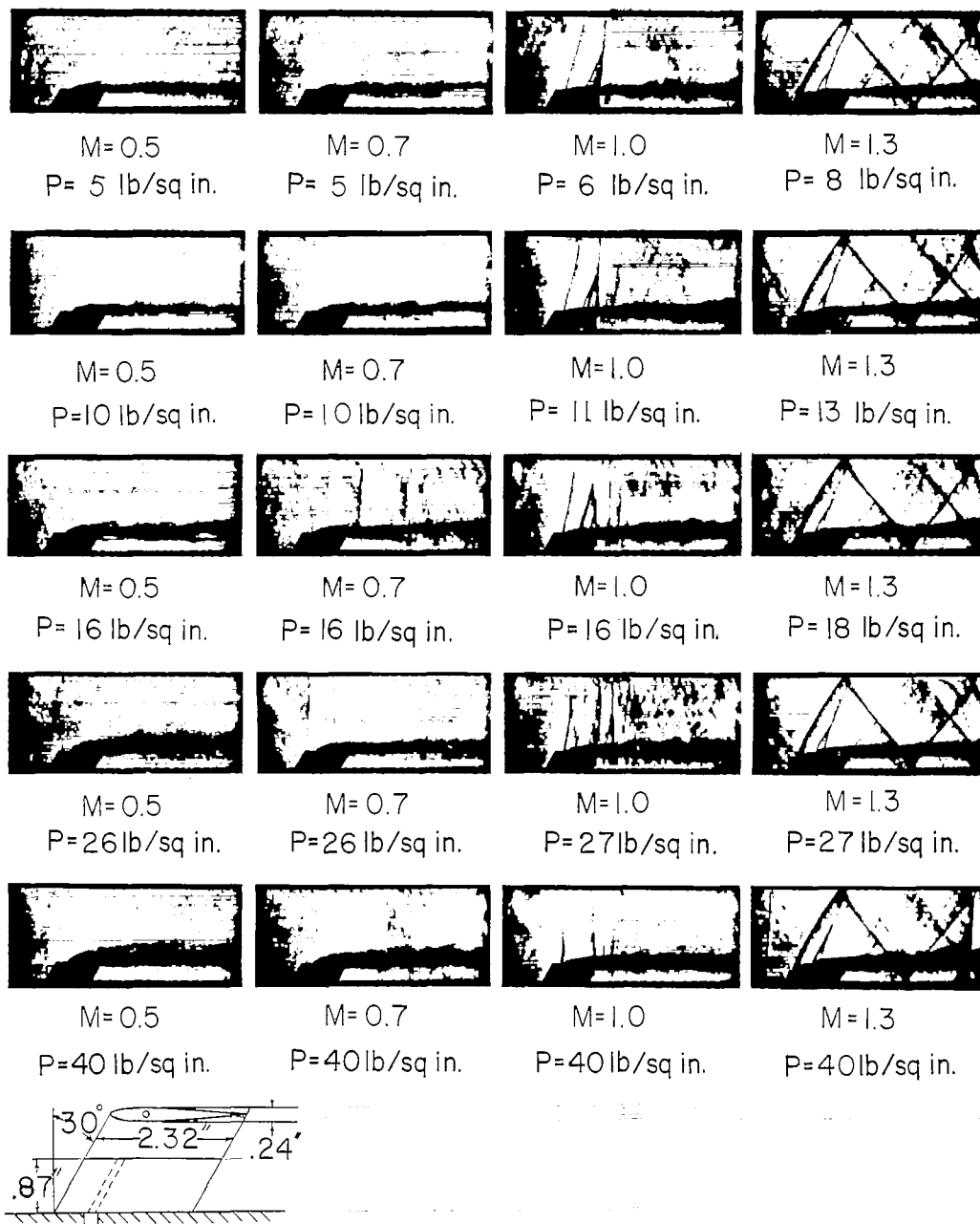
L-85614

Figure 8.- Concluded.

(a) $\Lambda = 0^\circ$; 1-inch extension.

L-85615

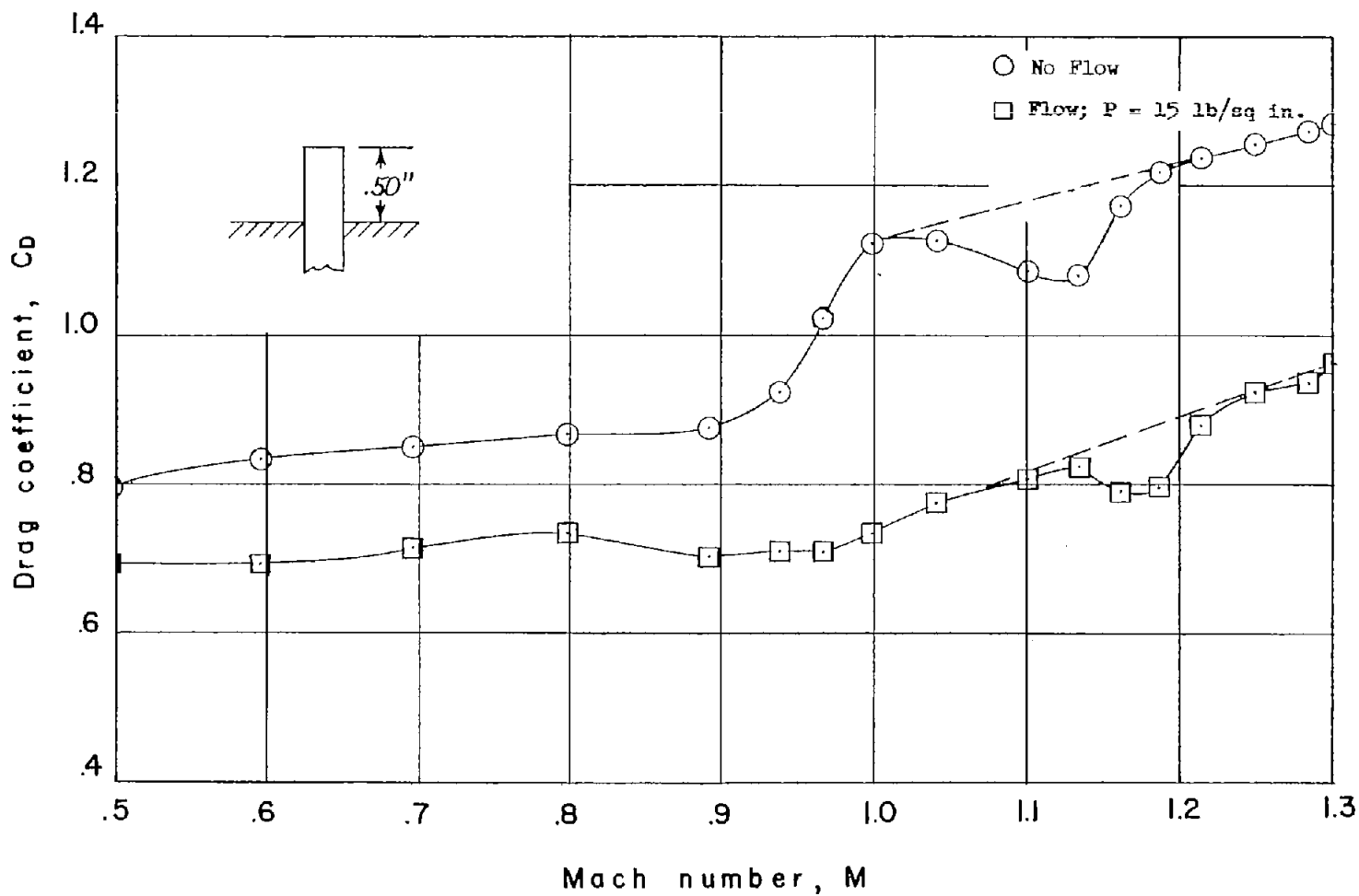
Figure 9.- Schlieren photographs of airfoil-shaped drain discharging liquid.



(b) $\Lambda = 30^\circ$; 0.87-inch extension (projected).

L-85616

Figure 9.- Concluded.



(a) $\Lambda = 0^\circ$; 0.50-inch extension.

Figure 10.- Variation of drag coefficient with Mach number for various cylindrical drains, with and without liquid flow.

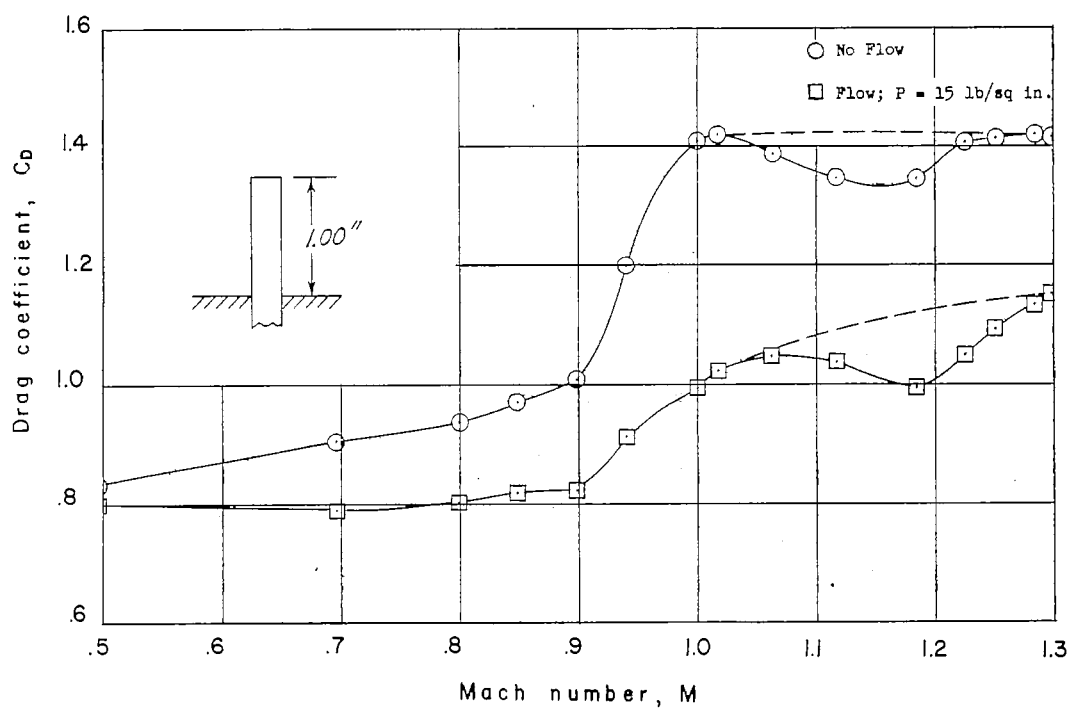
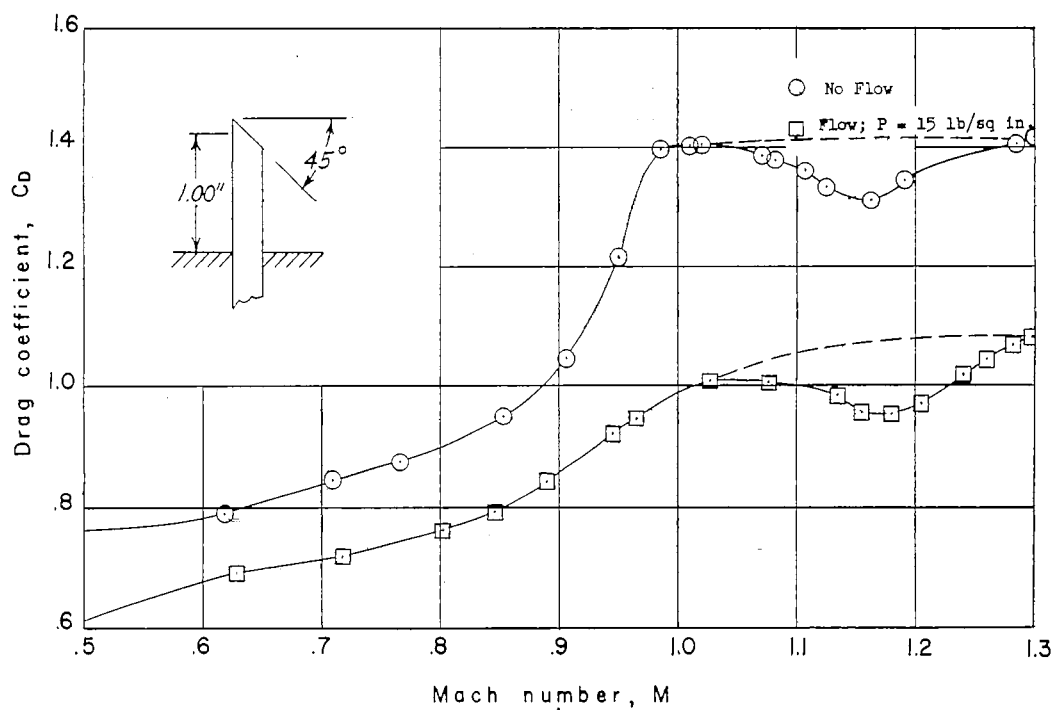
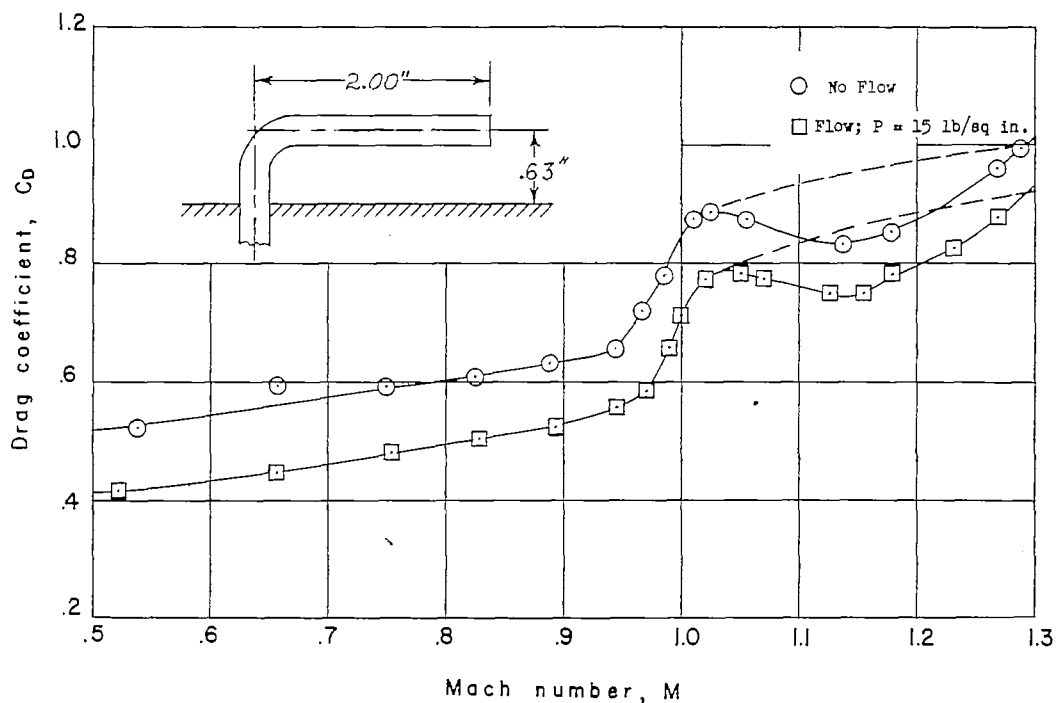
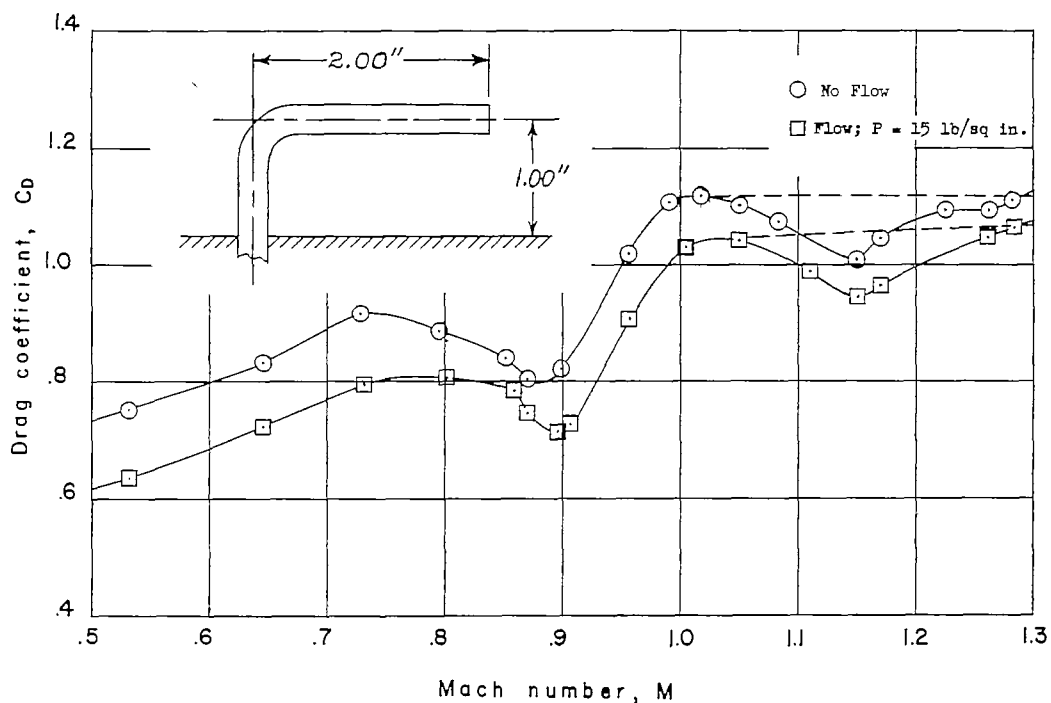
(b) $\Lambda = 0^\circ$; 1-inch extension.(c) $\Lambda = 0^\circ$; 1-inch extension; 45° chamfer.

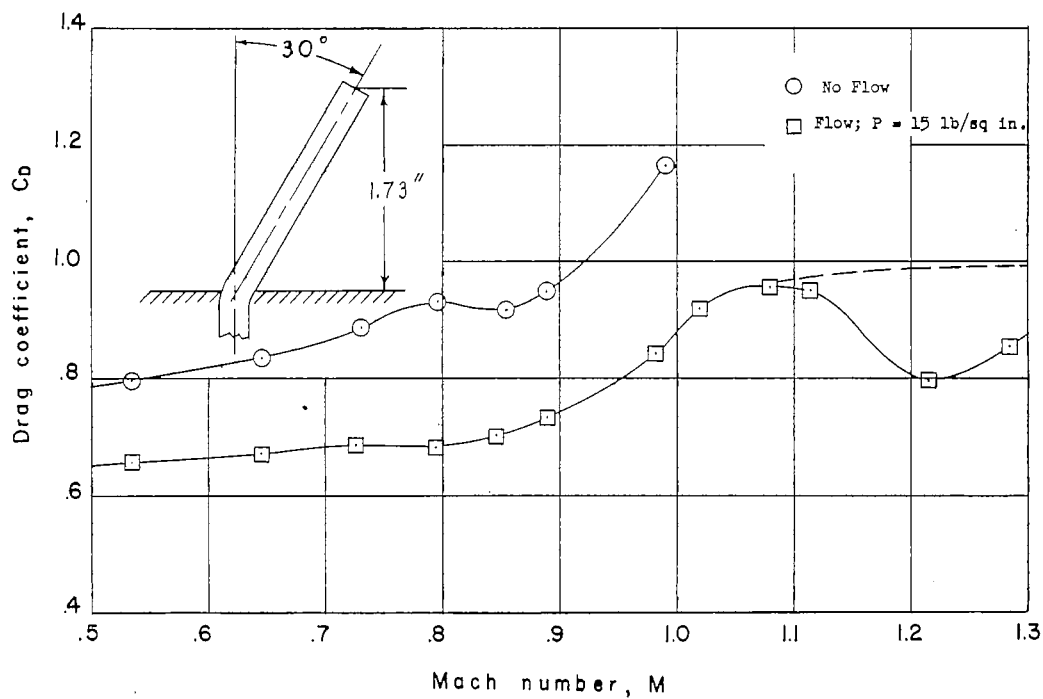
Figure 10.- Continued.



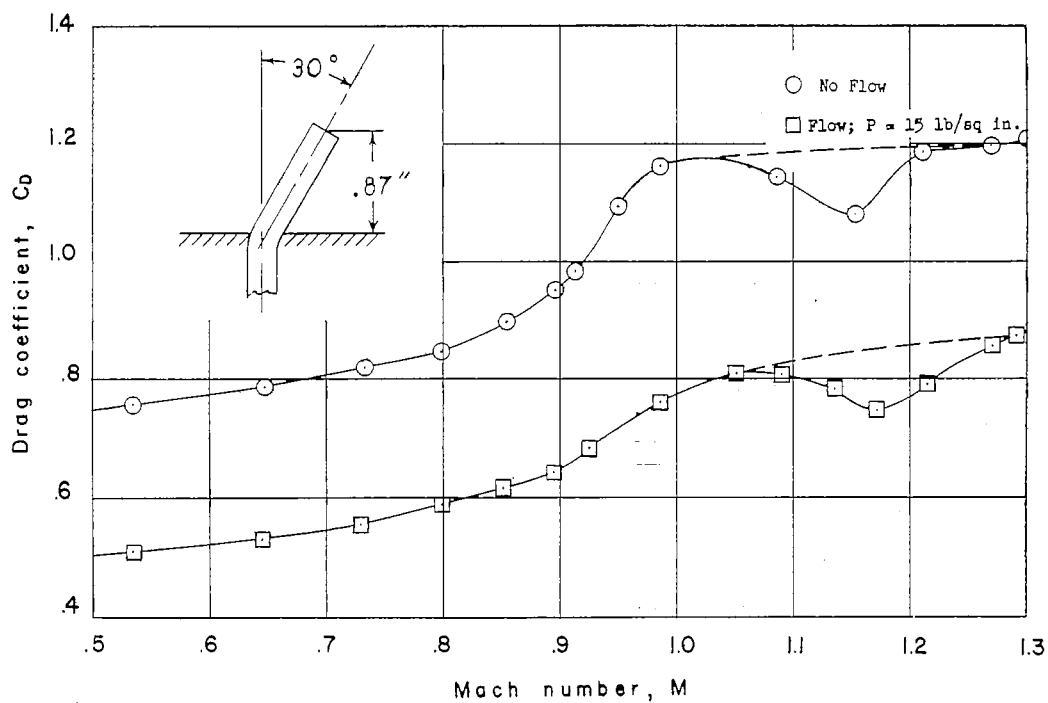
(d) $\Lambda = 0^\circ$; 0.63-inch extension; 90° bend; 2-inch straight section.



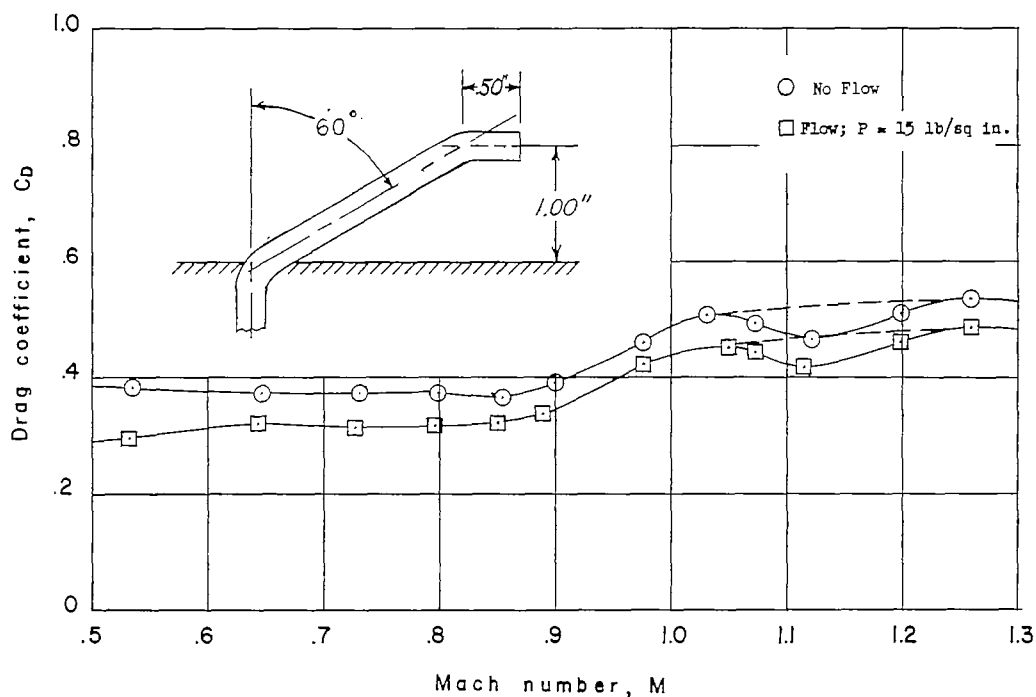
(e) $\Lambda = 0^\circ$; 1-inch extension; 90° bend; 2-inch straight section.



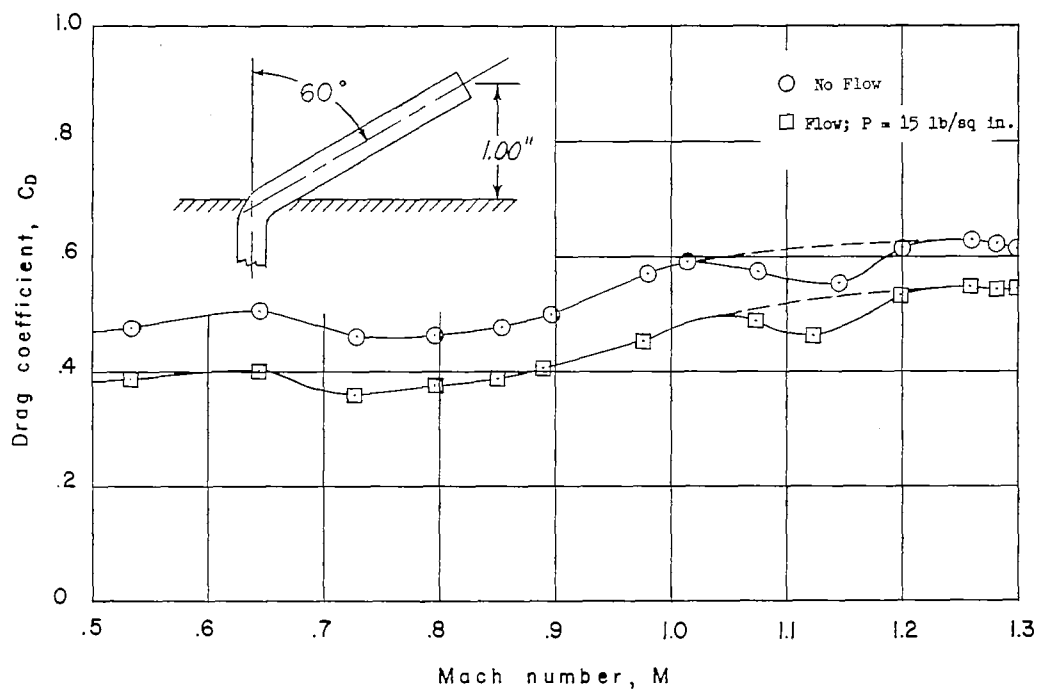
(f) $\Lambda = 30^\circ$; 1.73-inch extension (projected).



(g) $\Lambda = 30^\circ$; 0.87-inch extension (projected).

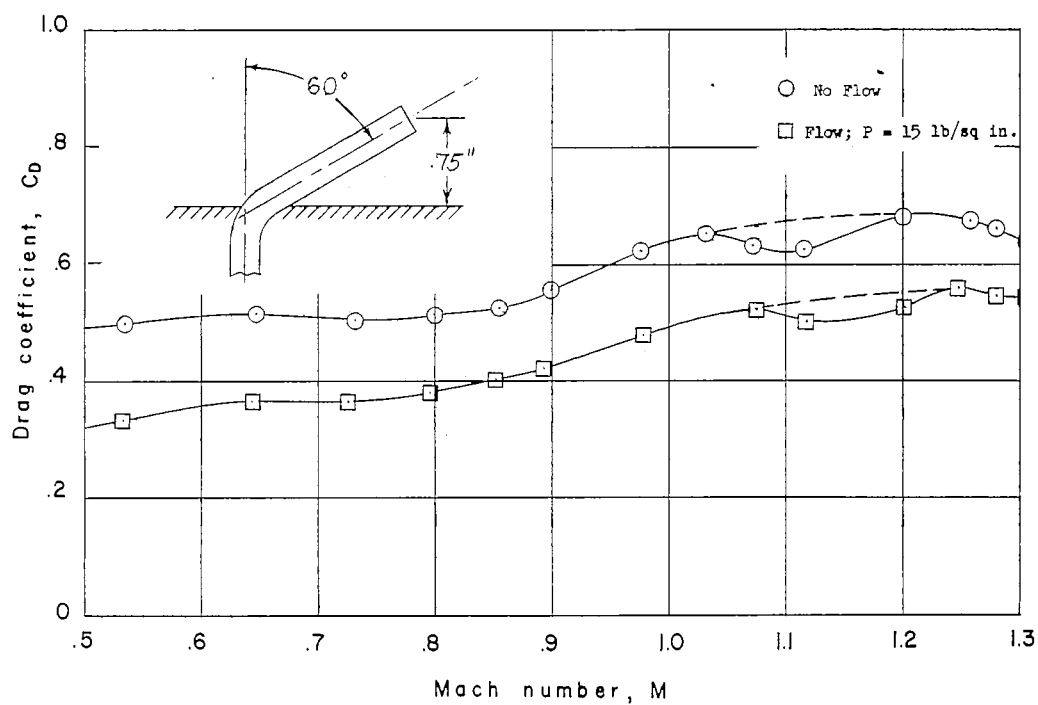


(h) $\Lambda = 60^\circ$; 1-inch extension (projected); 30° bend;
1/2-inch straight section.

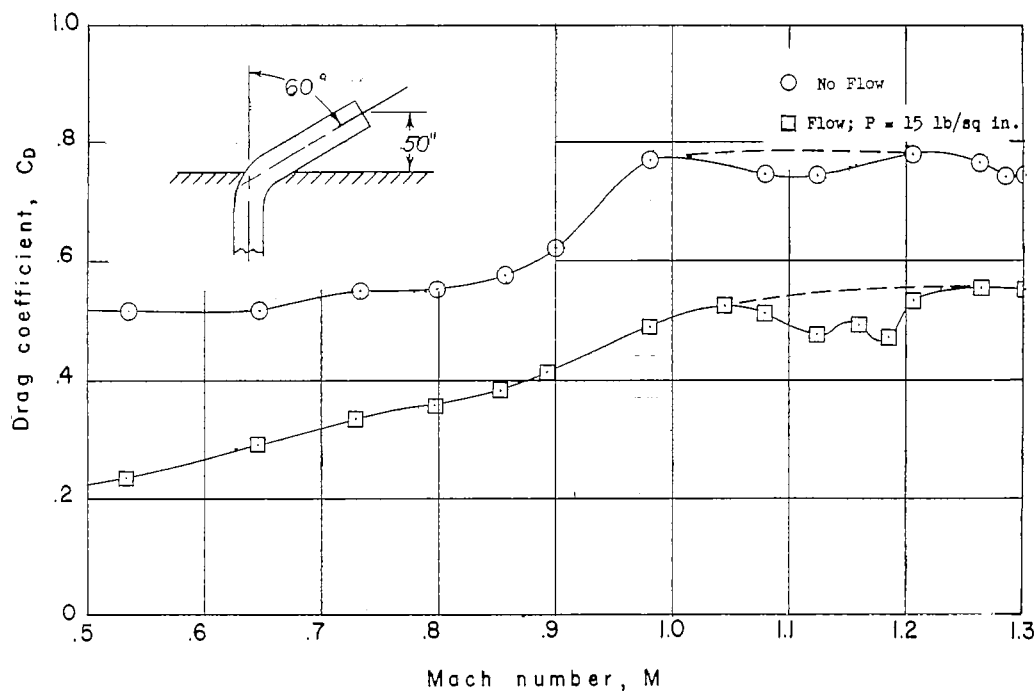


(i) $\Lambda = 60^\circ$; 1-inch extension (projected).

Figure 10.- Continued.

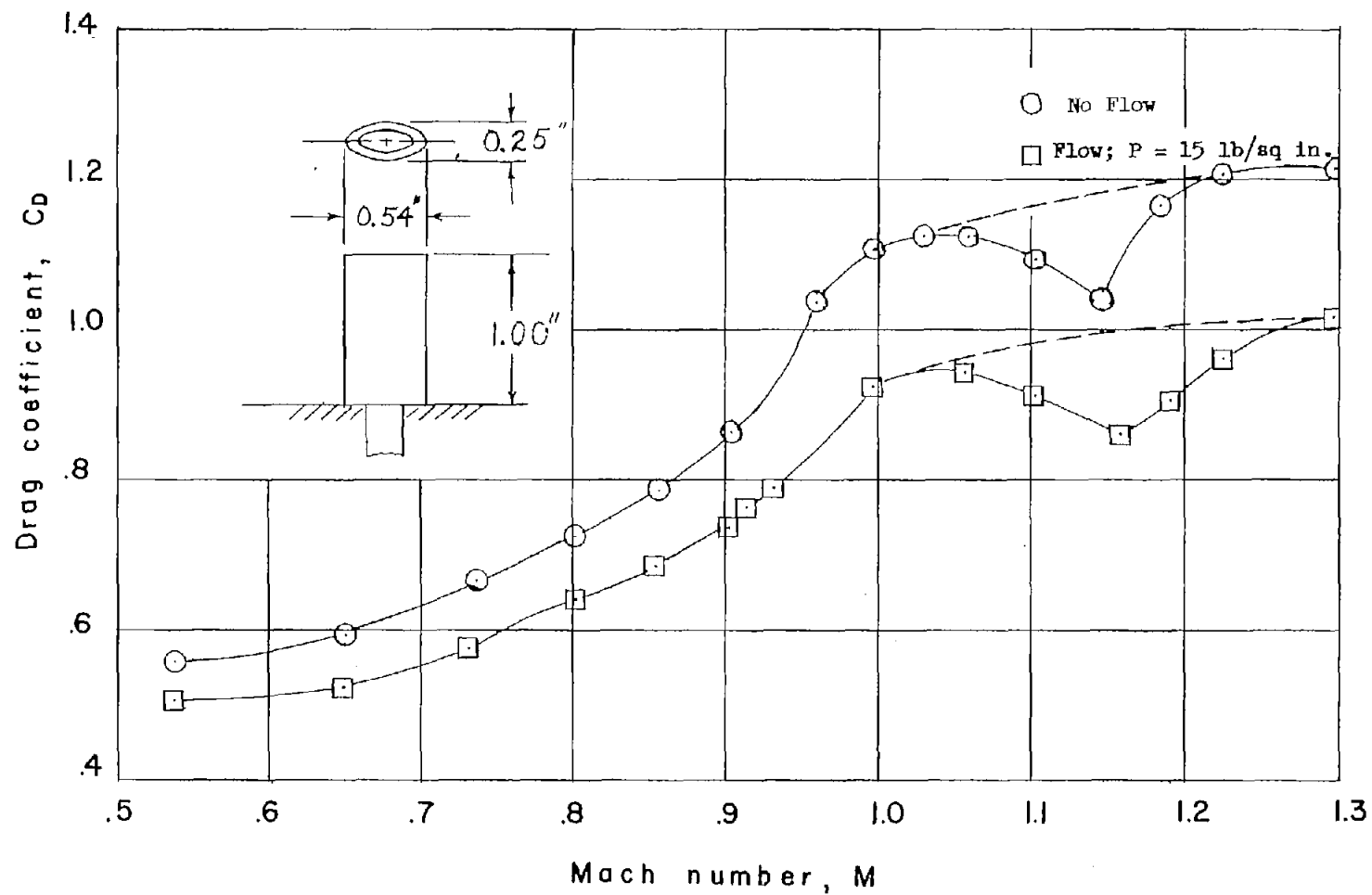


(j) $\Lambda = 60^\circ$; 0.75-inch extension (projected).



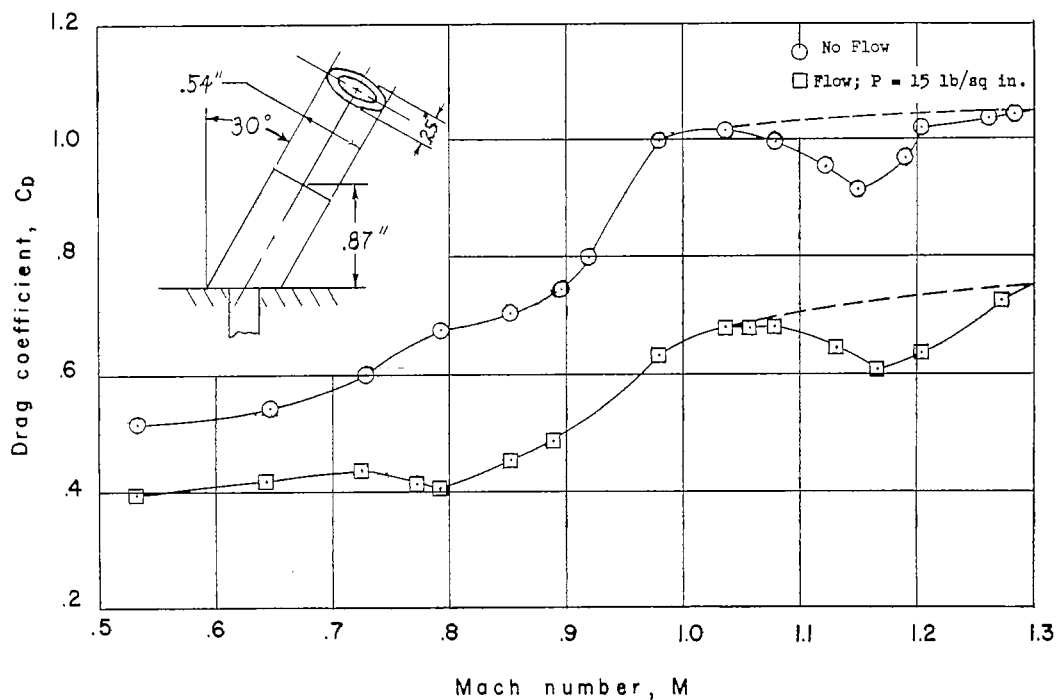
(k) $\Lambda = 60^\circ$; 0.50-inch extension (projected).

Figure 10.- Concluded.

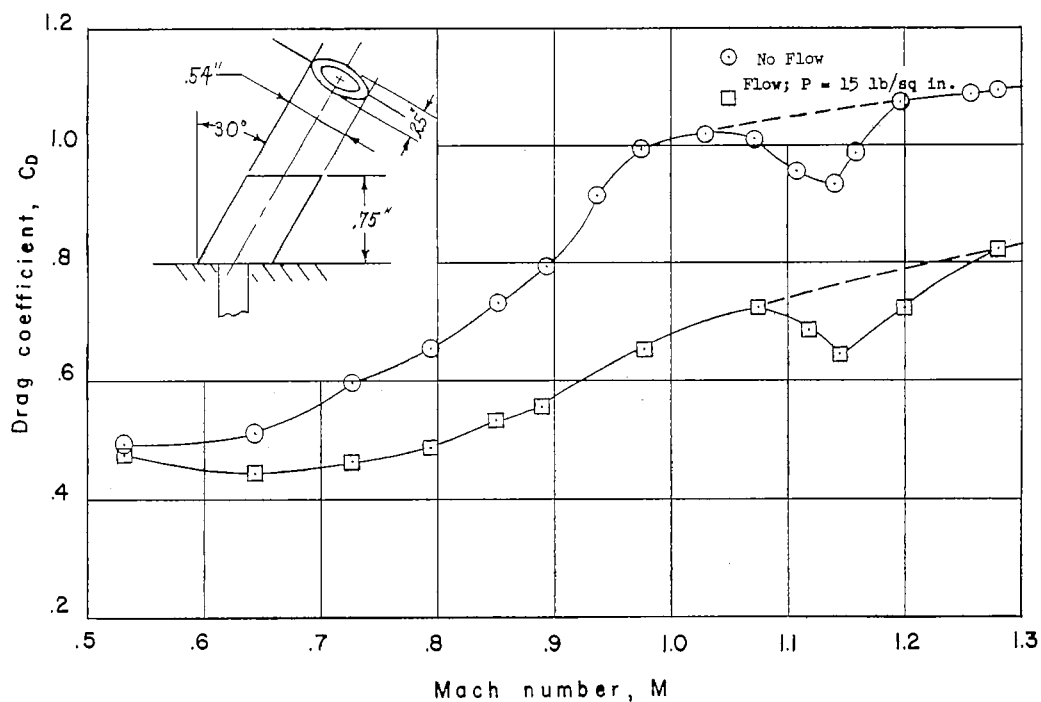


(a) $\Lambda = 0^\circ$; 1-inch extension.

Figure 11.- Variation of drag coefficient with Mach number for various elliptical drains, with and without liquid flow.

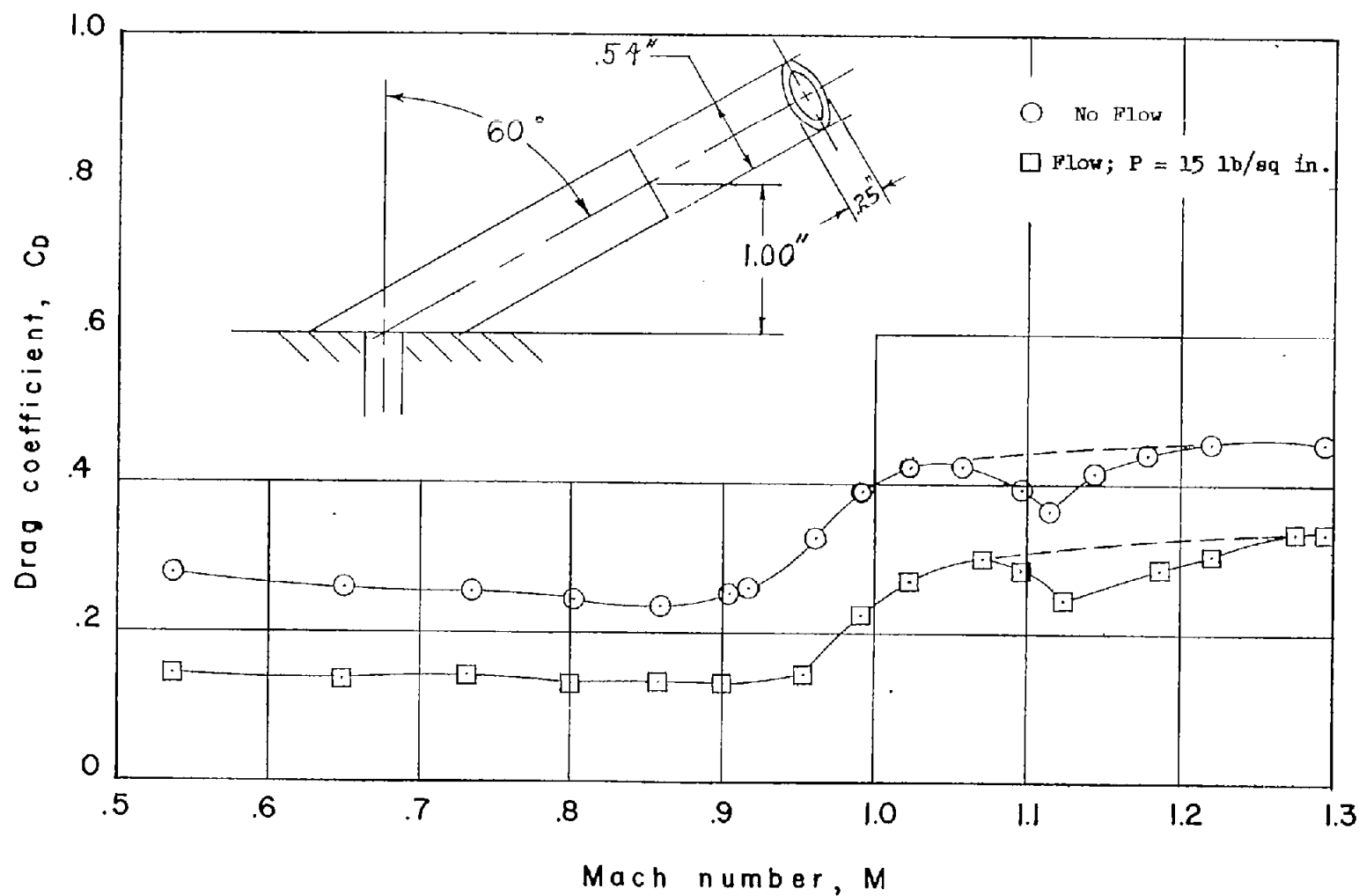


(b) $\Lambda = 30^\circ$; 0.87-inch extension (projected).



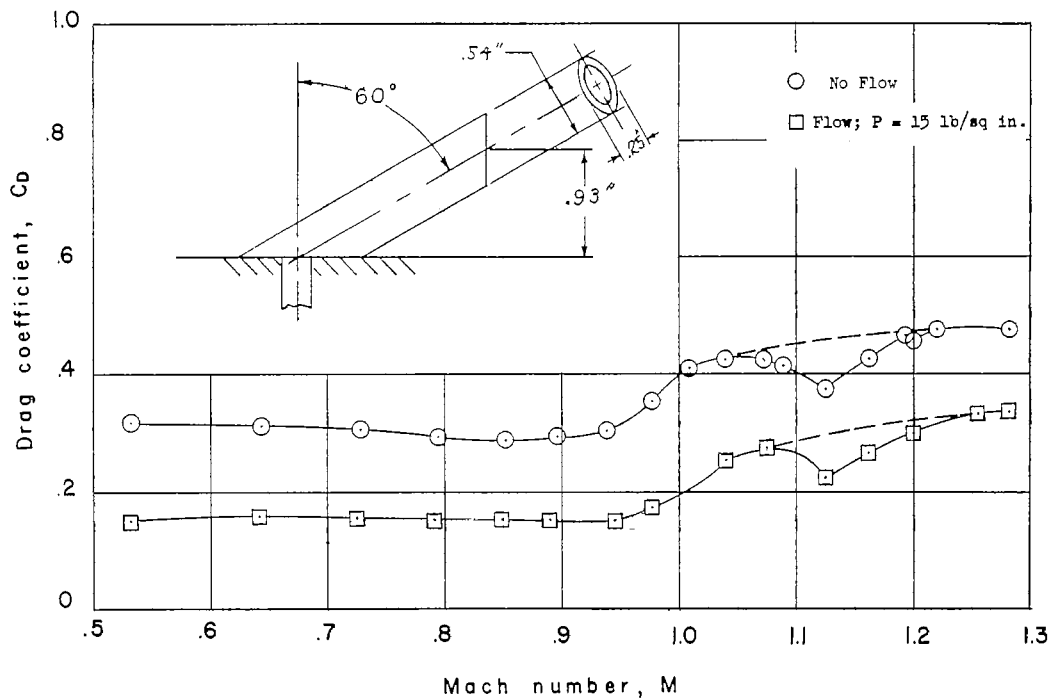
(c) $\Lambda = 30^\circ$; 0.75-inch extension (projected).

Figure 11.- Continued.

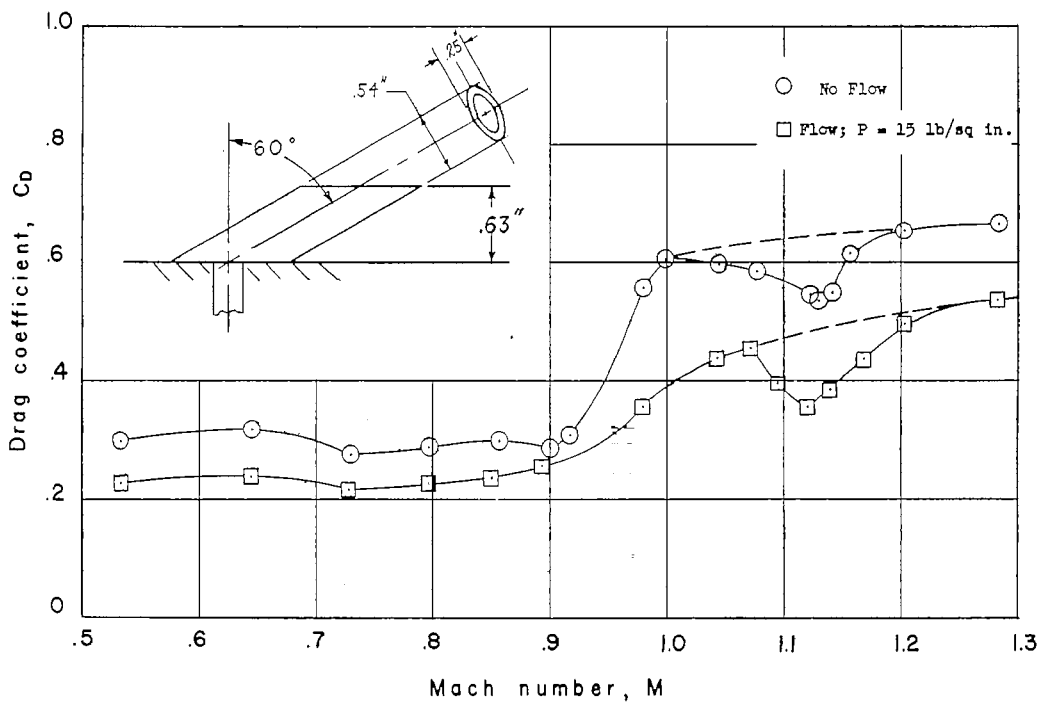


(d) $\Lambda = 60^\circ$; 1-inch extension (projected).

Figure 11.- Continued.

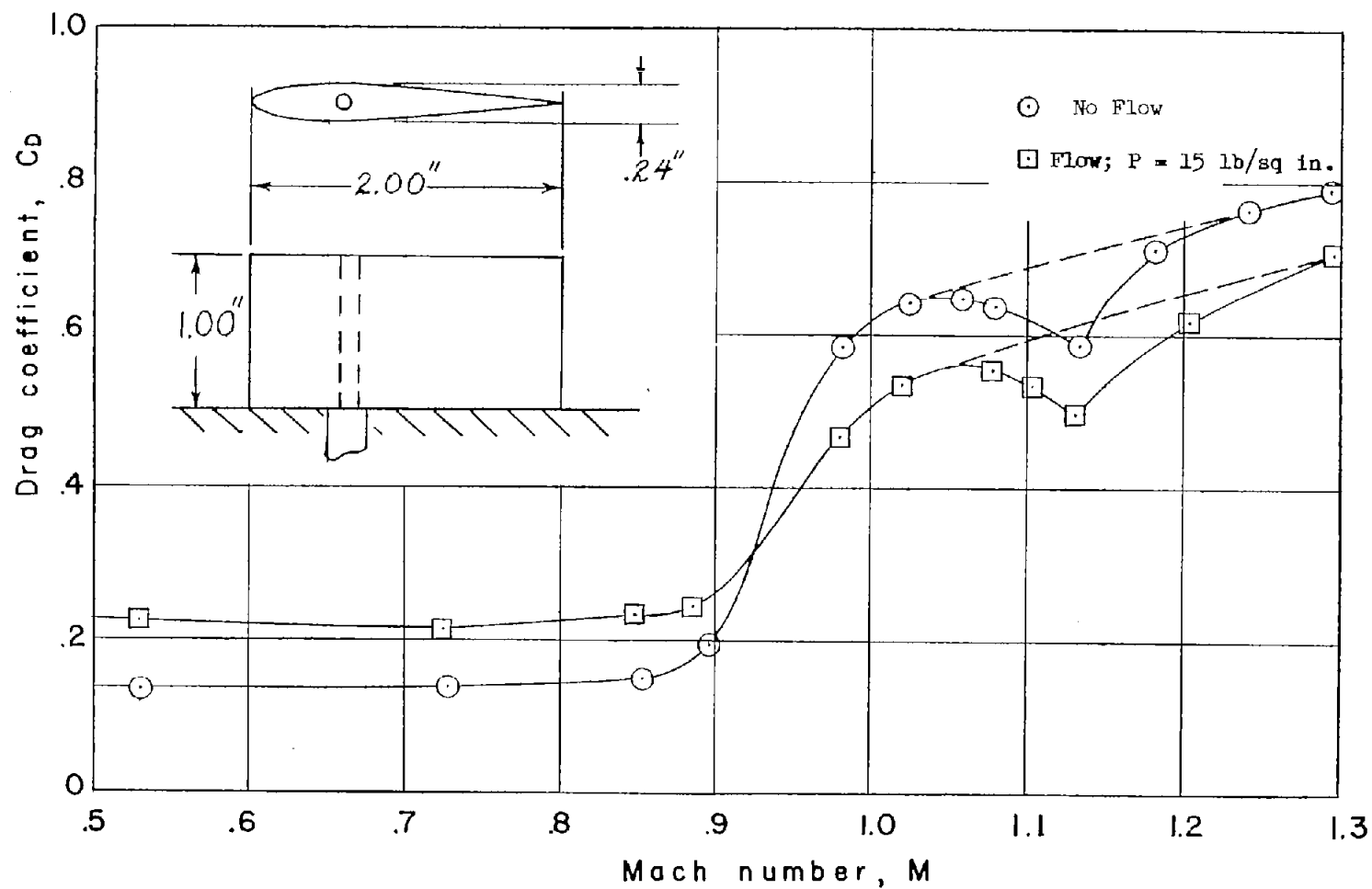


(e) $\Lambda = 60^\circ$; 0.93-inch extension (projected).



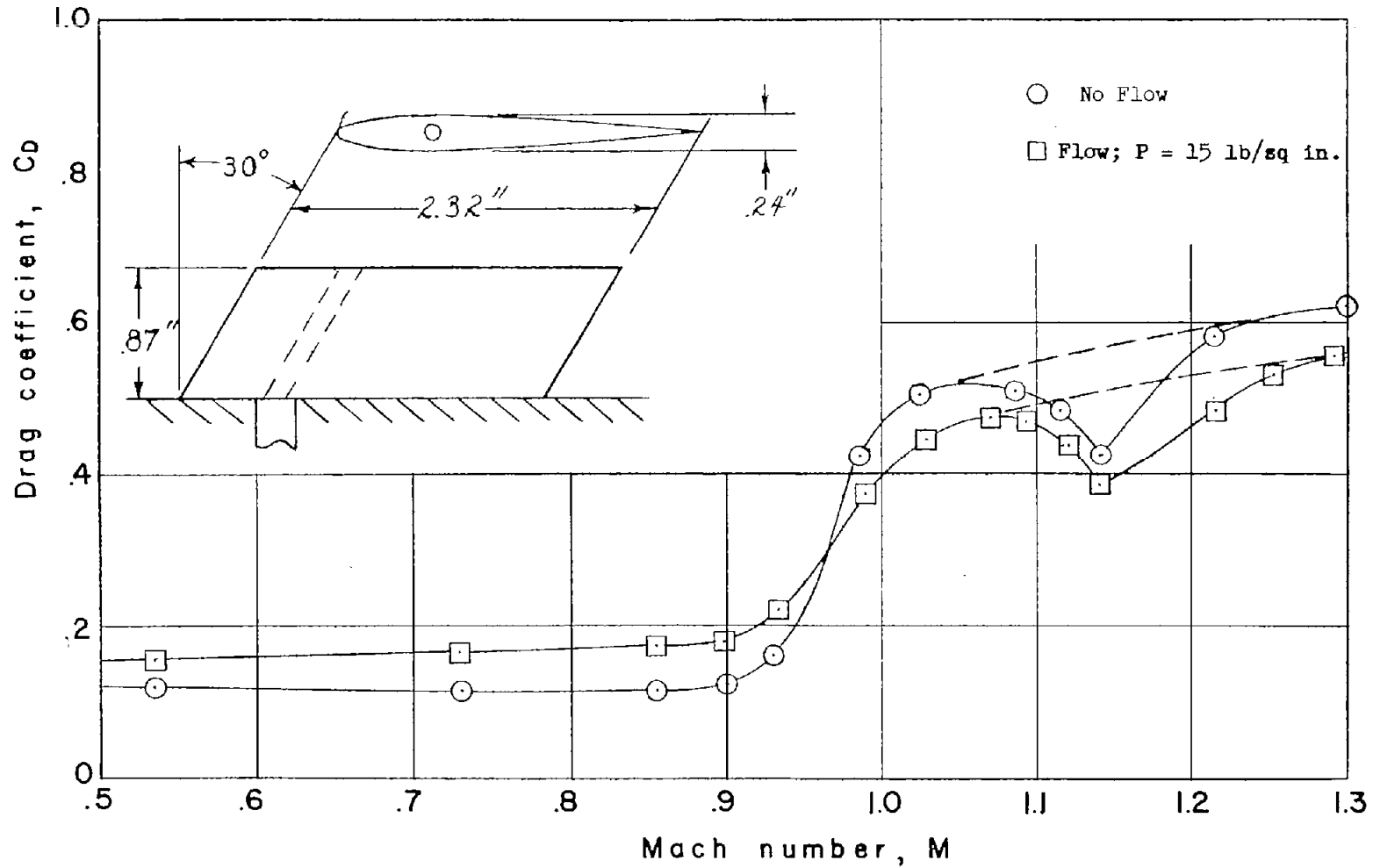
(f) $\Lambda = 60^\circ$; 0.63-inch extension (projected).

Figure 11.- Concluded.



(a) $\Lambda = 0^\circ$; 1-inch extension.

Figure 12.- Variation of drag coefficient with Mach number for airfoil-type drains, with and without liquid flow.



(b) $\Lambda = 30^\circ$; 0.87-inch extension (projected).

Figure 12.- Concluded.

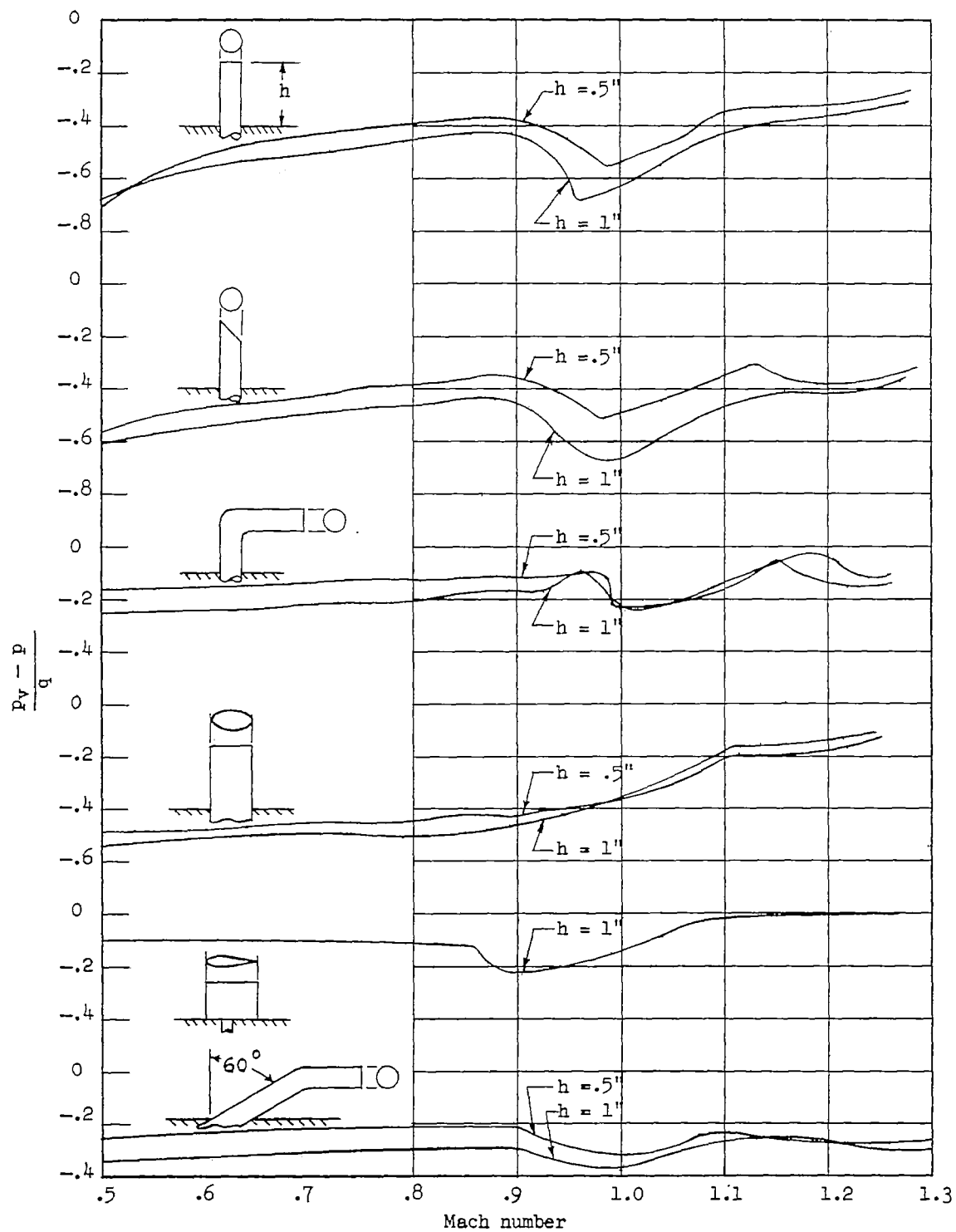


Figure 13.- Drain-vent, pressure coefficients.

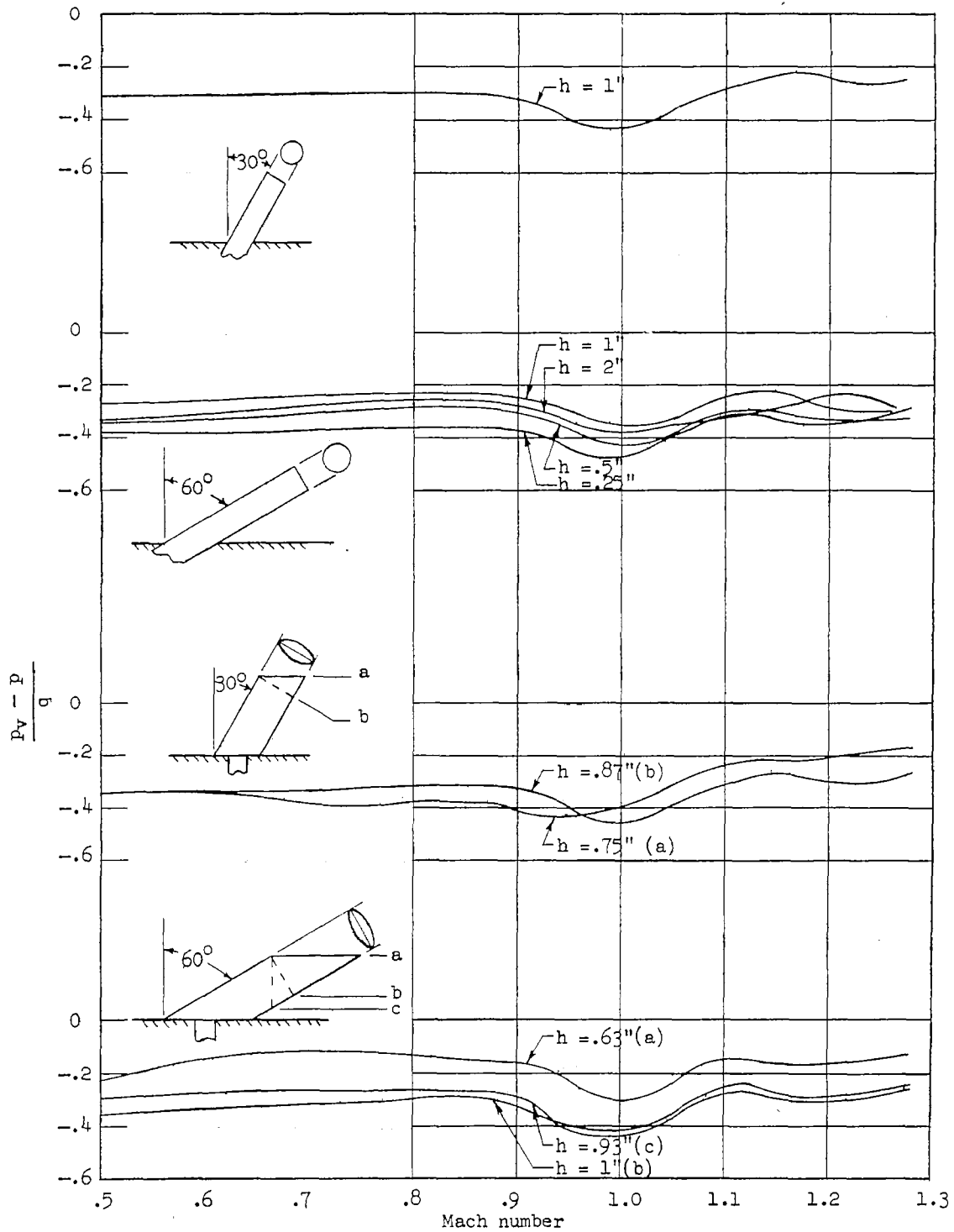


Figure 13.- Concluded.